

CONTRACT NO. NA35-9668

**NIMBUS-B SOLAR-CONVERSION
POWER SUPPLY SUBSYSTEM**

QUARTERLY TECHNICAL REPORT NO. 1
SEPTEMBER THROUGH NOVEMBER, 1965

Prepared for the

NATIONAL AERONAUTICS AND
SPACE ADMINISTRATION
WASHINGTON, D.C.

By the

ASTRO-ELECTRONICS DIVISION
DEFENSE ELECTRONIC PRODUCTS
RADIO CORPORATION OF AMERICA
PRINCETON, NEW JERSEY



AED R-2889

Issued: January 24, 1966

BLANK PAGE ii

BLANK PAGE iv

PREFACE

This is the first in a series of quarterly technical reports on the development of the Nimbus-B Solar-Conversion Power Supply Subsystem for the Nimbus Meteorological Satellite. This project is being conducted by the Astro-Electronics Division (hereafter called AED) of RCA for the National Aeronautics and Space Administration (NASA) under Contract No. NAS5-9668. The present report covers the work accomplished during the period of September through November, 1965.

TABLE OF CONTENTS

Section		Page
I	GENERAL	I-1
II	SYSTEMS CONSIDERATIONS	II-1
III	SOLAR-CELL ARRAY	III-1
	A. General	III-1
	B. Mean I-V Curve	III-1
	C. Radiation Damage Calculation	III-2
	D. Solar-Cell Design Factors	III-3
	E. Solar Cell I-V Calculation by Computer	III-3
	1. Computer Inputs	III-4
	2. Computer Output	III-4
IV	STORAGE BATTERIES	IV-1
	A. General	IV-1
	B. Analysis of General Electric Cell Data	IV-1
	C. Analysis of "Crane" Data	IV-3
	D. Preliminary "Parametric Study Curves" and Battery Module Estimated Current, Voltage, and Heat Generation	IV-6
V	BATTERY CONTROL AND PROTECTION CIRCUITS	V-1
	A. General	V-1
	B. Battery Charge Control	V-1
	1. General	V-1
	2. Region I Operation	V-2
	3. Region II Operation	V-3
	4. Region III Operation	V-4
	C. Telemetry Circuits	V-5
	D. Ground Commands	V-5

TABLE OF CONTENTS (Continued)

Section		Page
VI	ELECTRONICS MODULE.....	VI-1
	A. Electrical Design.....	VI-1
	B. Mechanical Design.....	VI-1
	1. General.....	VI-1
	2. Printed-Circuit Boards.....	VI-1
	3. Connectors and Wiring.....	VI-3
	4. Electromagnetic Compatibility.....	VI-4
	5. Weight.....	VI-5

LIST OF ILLUSTRATIONS

Figure		Page
II-1	Nimbus-B Power Supply Subsystem, Functional Block Diagram	II-3
II-2	Nimbus-B Electronics Module, Functional Block Diagram	II-5
II-3	Nimbus-B Battery Module, Functional Block Diagram	II-7
III-1	Solar Cell I-V Curve at Beginning of Life Cycle	III-7
III-2	Solar Cell I-V Curve After 6 Months of Life Cycle	III-9
III-3	Solar Cell I-V Curve After 9 Months of Life Cycle	III-11
III-4	Solar Cell I-V Curve After 12 Months of Life Cycle	III-13
IV-1	Nimbus-B Battery Cell Ampere-Hour Capacity Histograms	IV-2
IV-2	Average Cell Capacity (Ampere-Hours) Versus Temperature	IV-4
IV-3	Cell Capacity Frequency Distribution Histograms	IV-5
IV-4	General Electric Average Cell Voltage Versus Cycle	IV-6
IV-5	Gulton Average Cell Voltage Versus Cycle	IV-7
IV-6	Average Cell Voltage Versus Depth of Discharge and Temperature at 250 Cycles	IV-8
IV-7	Average Cell Voltage Versus Depth of Discharge and Temperature at 750 Cycles	IV-9
IV-8	Average Cell Voltage Versus Depth of Discharge and Temperature at 1250 Cycles	IV-10
IV-9	Average Cell Voltage Versus Depth of Discharge and Temperature at 1750 Cycles	IV-11
IV-10	Average Cell Voltage Versus Cycle at 20 Percent Depth of Discharge for General Electric Cells	IV-11
IV-11	Average Cell Voltage Versus Cycle at 20 Percent Depth of Discharge for Gulton Cells	IV-12
IV-12	Cell Charge and Discharge Voltages Versus Time at 25°C	IV-13
IV-13	Cell Charge and Discharge Voltages Versus Time at 25°C for 6 Months Cycling	IV-14
IV-14	Cell Charge and Discharge Voltages Versus Time at 25°C for 9 Months Cycling	IV-15
IV-15	Cell Charge and Discharge Voltages Versus Time at 25°C for 12 Months Cycling	IV-16
IV-16	Battery Module Estimated Current, Voltage, and Heat Generations Versus Time at 25°C	IV-17
V-1	Regions of Normal Charge Controller Operation	V-2
V-2	Current Regulator Block Diagram	V-3
V-3	Charge Controller Operation in Region II, Functional Diagram	V-3
V-4	Charge Controller Operation in High-Temperature Limit Mode (Region III)	V-5
V-5	Trickle-Charge Override Functional Diagram	V-7
V-6	Battery Disconnect Functional Diagram	V-7
VI-1	Proposed Nimbus-B Electronics Module Configuration	VI-2

LIST OF TABLES

Table		Page
III-1	Degradation Factors Due to Radiation	III-2
III-2	Solar Cell Worst-Case Design Factors	III-3
III-3	Solar Cell/Array Power Output Summary	III-5
IV-1	Summary of Battery Cell Frequency Distribution Data	IV-3
V-1	Battery Analog Signals for Telemetry Subsystem	V-6

SECTION I

GENERAL

The Nimbus-B Power Supply Subsystem consists of a solar-cell energy conversion array (divided between two support platforms), eight battery modules of nickel-cadmium storage cells, and an electronics module which contains the load-bus regulator and a group of electronic circuits designed for control, regulation, and protection of the power supply circuits, components, and telemetry data sensing. The solar-cell platforms are folded against the satellite during launch and are extended to expose the solar cells when the satellite is in orbit. The extension mechanisms lock after being fully extended; the platforms, however, will rotate to "follow" the sun. Each battery of 23 storage cells and its associated electronic circuitry are housed in a module casting with cover. These castings are located in the sensory subsystem structure of the satellite. The solar-array substrate, the solar-cell modules, and the storage module castings and covers are furnished to AED by NASA. The power supply development has been divided into various phases and tasks, all of which are covered in separate sections of this report.

During this period, AED accumulated system data necessary for performing an analysis of the Nimbus-B Power Supply Subsystem requirements. The information compiled includes:

- (1) Solar-array characteristics up to a one-year life cycle,
- (2) Estimated battery charge-discharge characteristics at 25°C,
- (3) Solar array predicted time-temperature profile, and
- (4) Power supply subsystem voltage drops and shunt losses.

The results of this system analysis will be covered in Quarterly Technical Report No. 2. Included in this report are the results of an analysis on the Nimbus-B solar-cell array. This analysis, based on theoretical and experimental data, covers:

- (1) Obtaining a mean I-V curve of a solar cell in a ten-cell module,
- (2) Estimated flux degradation factors due to radiation,
- (3) Solar cell worst-case design factors, and
- (4) Solar cell I-V calculation by computer.

Three areas of study in the development of the Nimbus-B storage battery are covered in this report. This study, conducted at AED, involved:

- (1) An analysis of General Electric data on Nimbus type storage cells made for NASA,
- (2) An analysis of acceptance test and cycling program data for a group of General Electric and Gulston cells submitted by NASA to the U. S. Naval Quality Evaluation Laboratory at Crane, Indiana, and
- (3) Preparation of preliminary "parametric study" curves, and battery module estimated current, voltage, and heat generation.

In connection with above, a description of the battery control and protection circuits is also included in this report. These circuits, presently in the development stages, are an integral part of the battery module. The battery control and protection circuits provide control of the recharging of the nickel-cadmium battery; analog signals as a function of battery parameters for the spacecraft telemetry subsystem; and a means for executing certain ground signals received from the spacecraft command subsystem.

The electrical and mechanical designs for the Nimbus-B electronics module, including module packaging concept and component arrangement, were completed and are covered in this report. Preliminary RFI testing and EMI investigations were completed on a newly assembled electronics module breadboard model.

SECTION II

SYSTEMS CONSIDERATIONS

Functional block diagrams have been prepared for the power supply subsystem, the electronics module, and the battery module. These diagrams are shown in Figures II-1, II-2, and II-3, respectively.

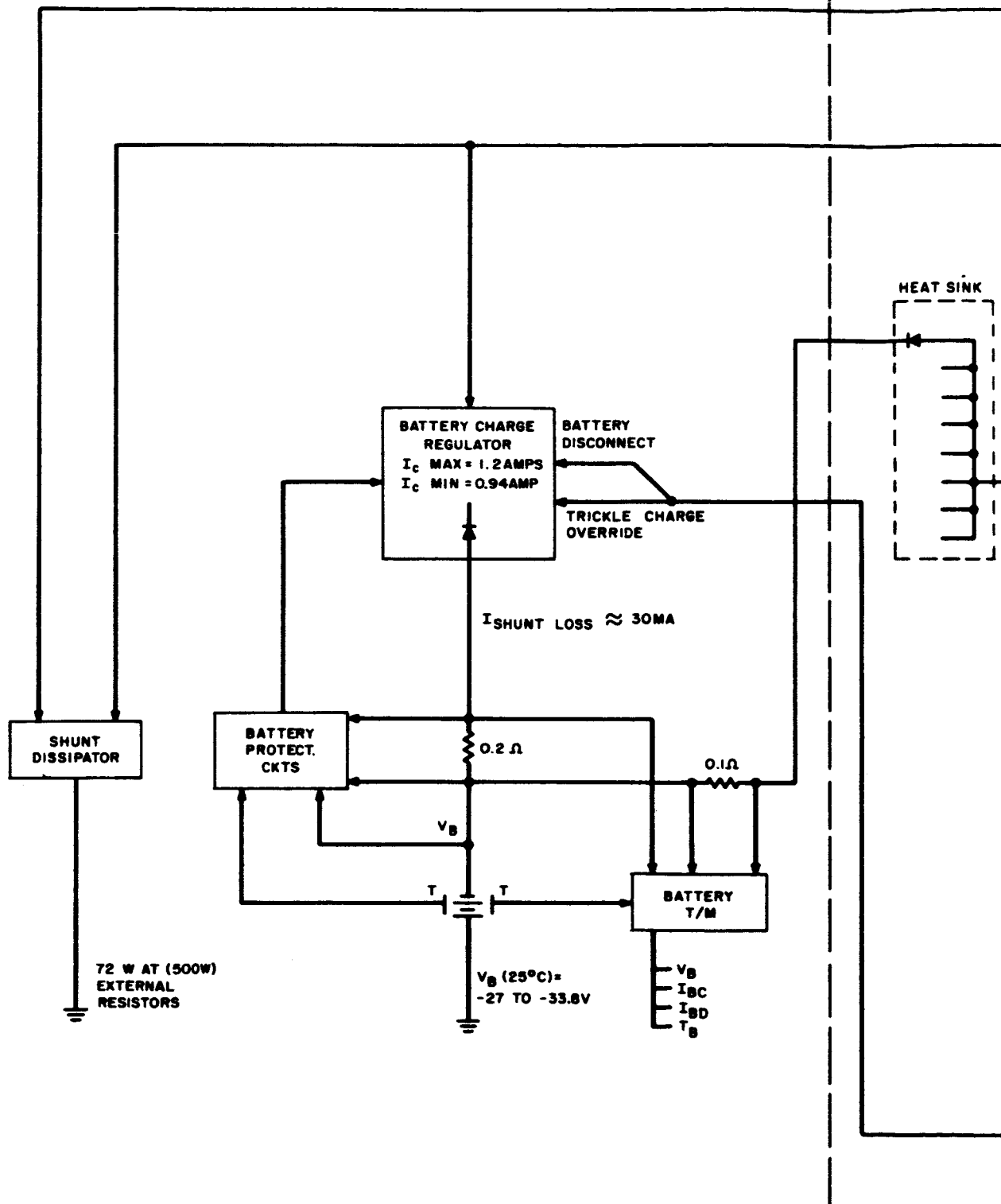
The existing energy-balance computer program has been modified to more accurately simulate the effects of degradation and temperature on the solar-array characteristics. Debugging of the program is in process.

The information required for the power supply subsystem analysis has been accumulated. This includes the following:

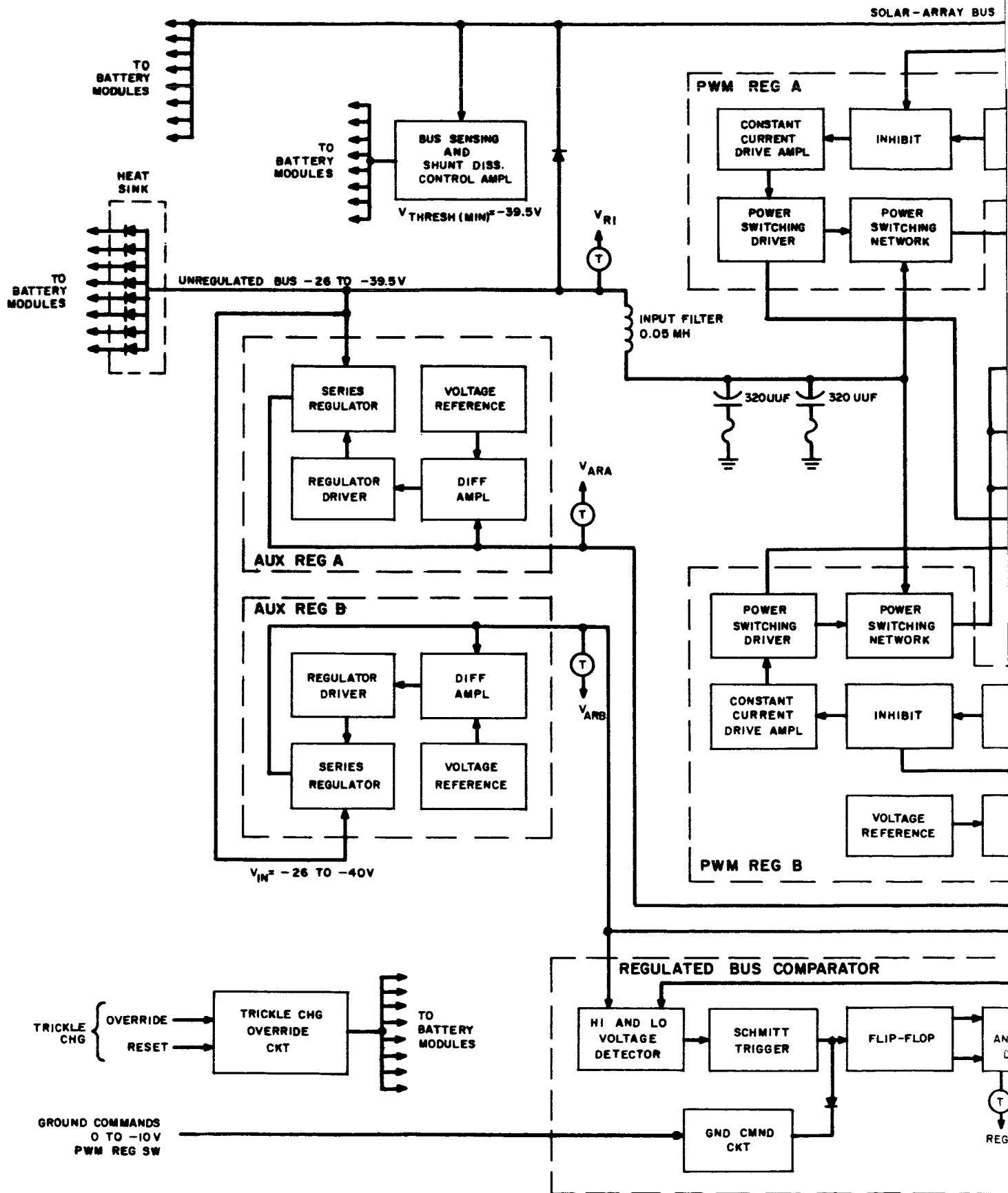
- (1) Solar-array characteristics at beginning of life and at six, nine, and 12 months;
- (2) Estimated battery charge-discharge characteristics at 25°C;
- (3) Solar array predicted time-temperature profile; and
- (4) Power supply subsystem voltage drops and shunt losses.

The results of the system analysis will appear in Quarterly Technical Report No. 2.

BATTERY MODULE



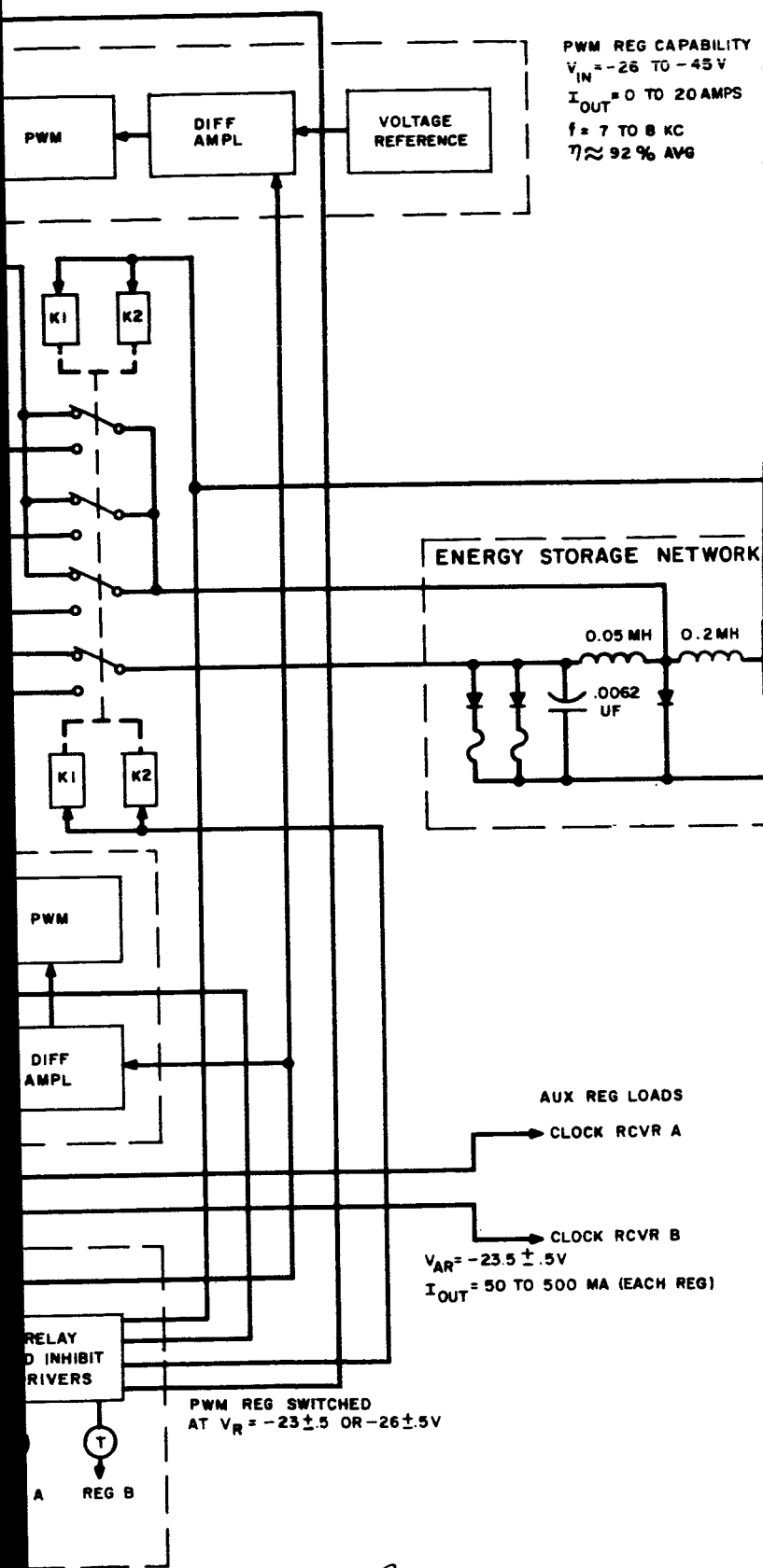
IL-3



II-5

1

0 TO -40V



PWM REG CAPABILITY
 $V_{IN} = -26$ TO $-45V$
 $I_{OUT} = 0$ TO 20 AMPS
 $f = 7$ TO 8 KC
 $\eta \approx 92\%$ AVG

ENERGY STORAGE NETWORK

0.05 MH 0.2 MH

.0062 UF

AUX REG LOADS

CLOCK RCVR A

CLOCK RCVR B

$V_{AR} = -23.5 \pm .5V$

$I_{OUT} = 50$ TO 500 MA (EACH REG)

PWM REG SWITCHED
AT $V_R = -23 \pm .5$ OR $-26 \pm .5V$

RELAY AND INHIBIT DRIVERS
A REG B

2

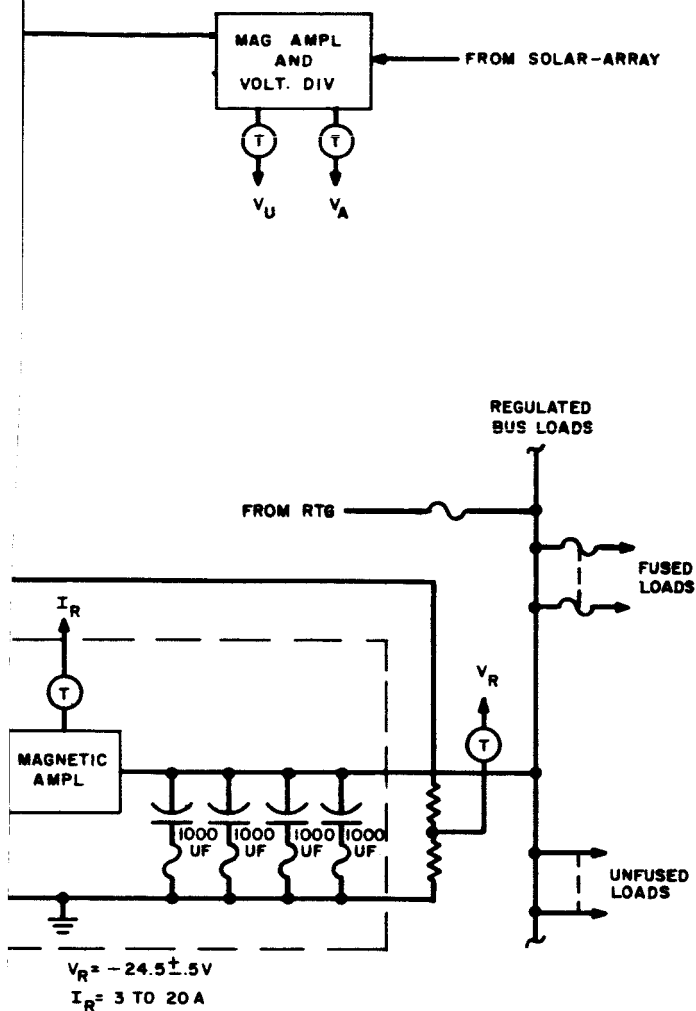


Figure II-2. Nimbus-B Electronics Module, Functional Block Diagram

3

ELECTRONICS MODULE

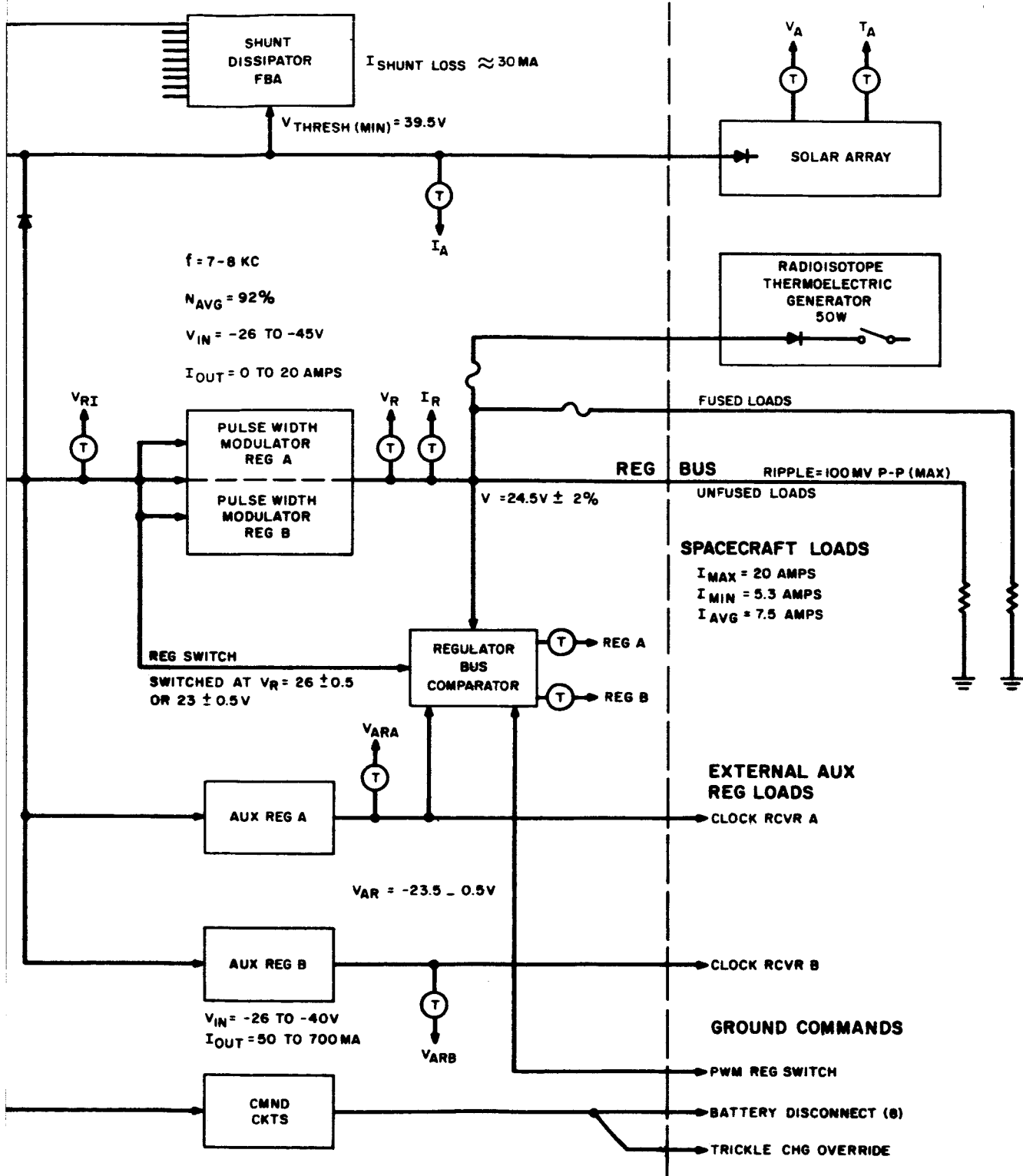
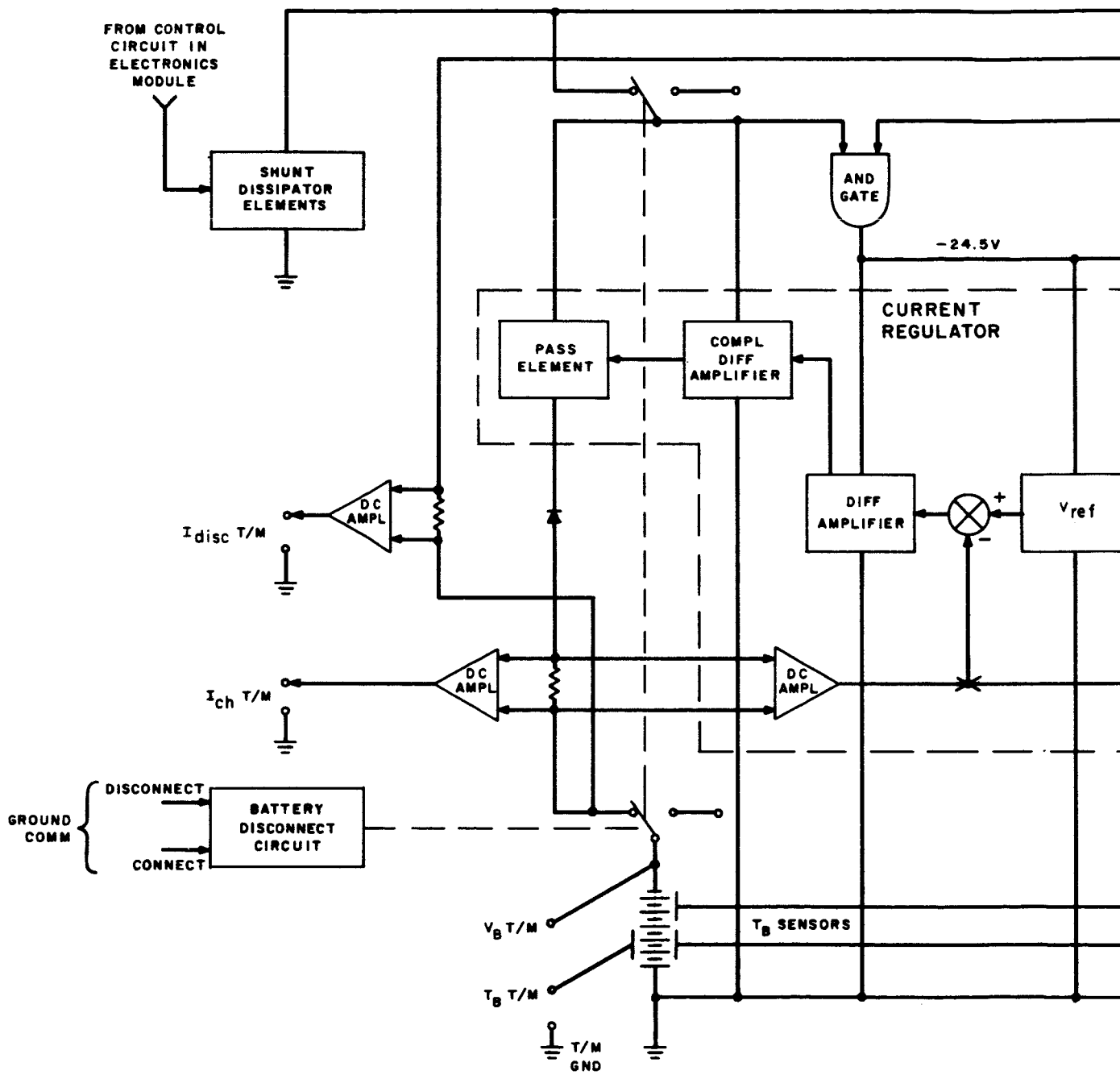
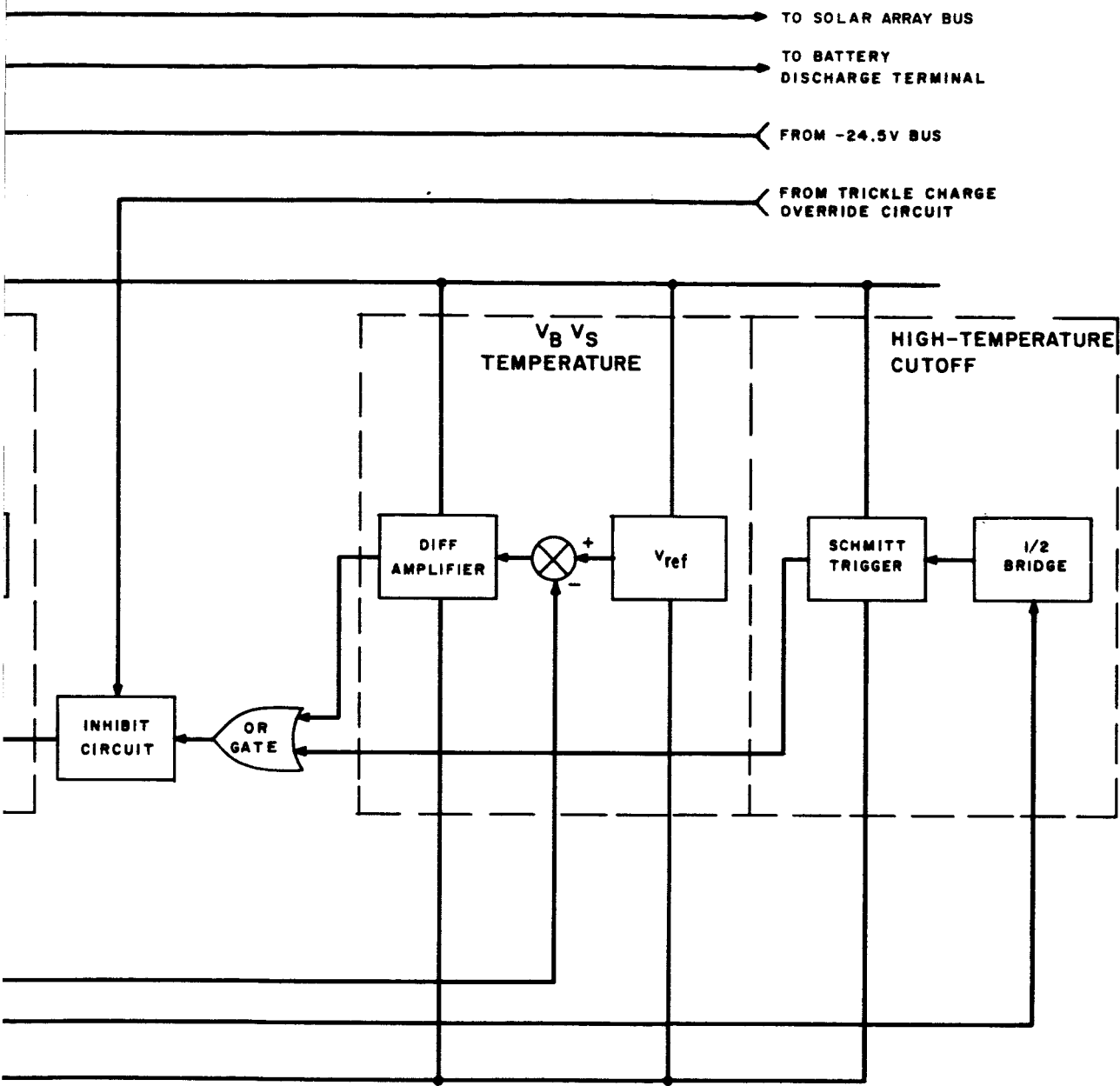


Figure II-1. Nimbus-B Power Supply Subsystem, Functional Block Diagram



II-7



2

Figure II-3. Nimbus-B Battery Module Functional Block Diagram

SECTION III
SOLAR-CELL ARRAY

A. GENERAL

In order to determine the optimum series-parallel combination of solar-cell modules, the following analyses were performed:

- Mean I-V curve of modularized cell from data taken at RCA Mountaintop, Pa., and recorded on the module travel tags;
- Electron and proton flux data for the Nimbus orbit;
- Conversion of raw flux data to damage equivalent 1 Mev electron flux, and calculation of the resulting degradation to the cell; and
- Calculation of the I-V curve of a cell in an array at various points in the mission for various temperatures.

B. MEAN I-V CURVE

The results of a statistical analysis are presented below for the mean I-V curve of a cell in a ten-cell module:

- | | | |
|------------------------------|---|-------------|
| (1) Short-circuit current | - | 134.0 ma |
| (2) Current at maximum power | - | 118.5 ma |
| (3) Voltage at maximum power | - | 0.470 volt |
| (4) Open-circuit voltage | - | 0.5945 volt |

The conditions under which the above parameters were determined are as follows:

- 136.6 mw/cm^2 tungsten equivalent air-mass-zero intensity as determined by Nimbus standard solar cells.*
- $25 \pm 2^\circ\text{C}$ temperature.
- Tungsten 500-watt lamps generated at a color temperature of 2800°K .

*See standard cell tolerances under design factors.

C. RADIATION DAMAGE CALCULATION

Two estimates of raw flux were obtained, the flux of electrons and protons projected to 1968 and the flux for 1963. The difference in the two flux estimates is due to the exponential decay of the artificial electron belt introduced by the Starfish test of July 1962. Since the modules are furnished by NASA and are already fabricated, and since the panels are already fabricated, the 1968 flux estimate was used in determining the number of series-parallel cells. (In addition, verbal direction was given by NASA to use the 1968 flux estimates.) The damage equivalent 1 Mev electron flux is defined below:

	<u>6 Months</u>	<u>9 Months</u>	<u>1 Year</u>
1963	4.06×10^{12}	6.1×10^{14}	8.13×10^{14}
1968	1.3×10^{14}	1.95×10^{14}	2.6×10^{14}

The degradation factors using the two fluxes is defined in Table III-1.

TABLE III-1. DEGRADATION FACTORS DUE TO RADIATION

Current-Voltage Power	6 Months		9 Months		1 Year	
	1963 Flux	1968 Flux	1963 Flux	1968 Flux	1963 Flux	1968 Flux
Short-Circuit Current	0.860	0.920	0.835	0.901	0.815	0.885
Maximum Power Current	0.860	0.920	0.835	0.901	0.815	0.885
Maximum Power Voltage	0.935	0.960	0.925	0.953	0.918	0.946
Open-Circuit Voltage	0.920	0.948	0.910	0.937	0.903	0.931
P _{max}	0.804	0.883	0.772	0.859	0.748	0.837

The difference in power available between the 1968 and 1963 fluxes is easily calculated by:

$$\frac{P_{\max} \text{ 1 year (1968)}}{P_{\max} \text{ 1 year (1963)}} = \frac{0.837}{0.748} = 1.12,$$

or 12 percent more power is available at the end of life using 1968 flux.

D. SOLAR CELL DESIGN FACTORS

The solar cell design factors listed in Table III-2 are based upon theoretical and/or experimental data.

TABLE III-2. SOLAR CELL WORST-CASE DESIGN FACTORS

Design Factors	First Day Design Worst Case	6 Months Worst Case	9 Months Worst Case	12 Months Worst Case
<u>Current:</u>				
Ultra Violet to Cover Glass and Adhesive	0.95	0.95	0.95	0.95
Standard Cell Tolerance	0.902	0.902	0.902	0.902
Current Measurement Tolerance	0.98	0.98	0.98	0.98
Solar Constant	0.965	0.965	0.965	0.965
$\frac{139.6}{136.6}$ - Since the modules were measured at 136.6 mv/cm ² *	1.022	1.022	1.022	1.022
<u>Voltage:</u>				
Voltage Measurement Uncertainty	0.98	0.98	0.98	0.98
Series Resistance	0.98	0.98	0.98	0.98
Thermal Cycling	1.0	0.982	0.982	0.982
*Tungsten equivalent air-mass-zero intensity				

E. SOLAR CELL I-V CALCULATION BY COMPUTER

A computer program was utilized to obtain an I-V curve of a solar cell in an array (before the blocking diodes) at various points in the mission and at the desired temperatures.

1. COMPUTER INPUTS

- (a) Design factors - current and voltage,
- (b) Maximum power voltage, undegraded cell,
- (c) Maximum power current, undegraded cell,
- (d) Open-circuit voltage, undegraded cell,
- (e) Temperature of input I-V curve,
- (f) Current temperature coefficient 0.000061 amp/°C,
- (g) Voltage temperature coefficient 0.0022 volt/°C,
- (h) Temperatures at which fully degraded I-V curves are desired, and
- (i) I-V curve of cell that has been degraded for radiation damage.

2. COMPUTER OUTPUT

Fully degraded I-V curves at desired temperatures were developed from the computer output in the following manner:

- (1) Print out in 20 mv increments of degraded cell I-V curve, and
- (2) Plot of cell I-V curves.

The results of the analyses are summarized in Table III-3 for the worst case at 40°C (except for radiation damage where 1968 fluxes were used). The average array temperature in sunlight is 40° centigrade.

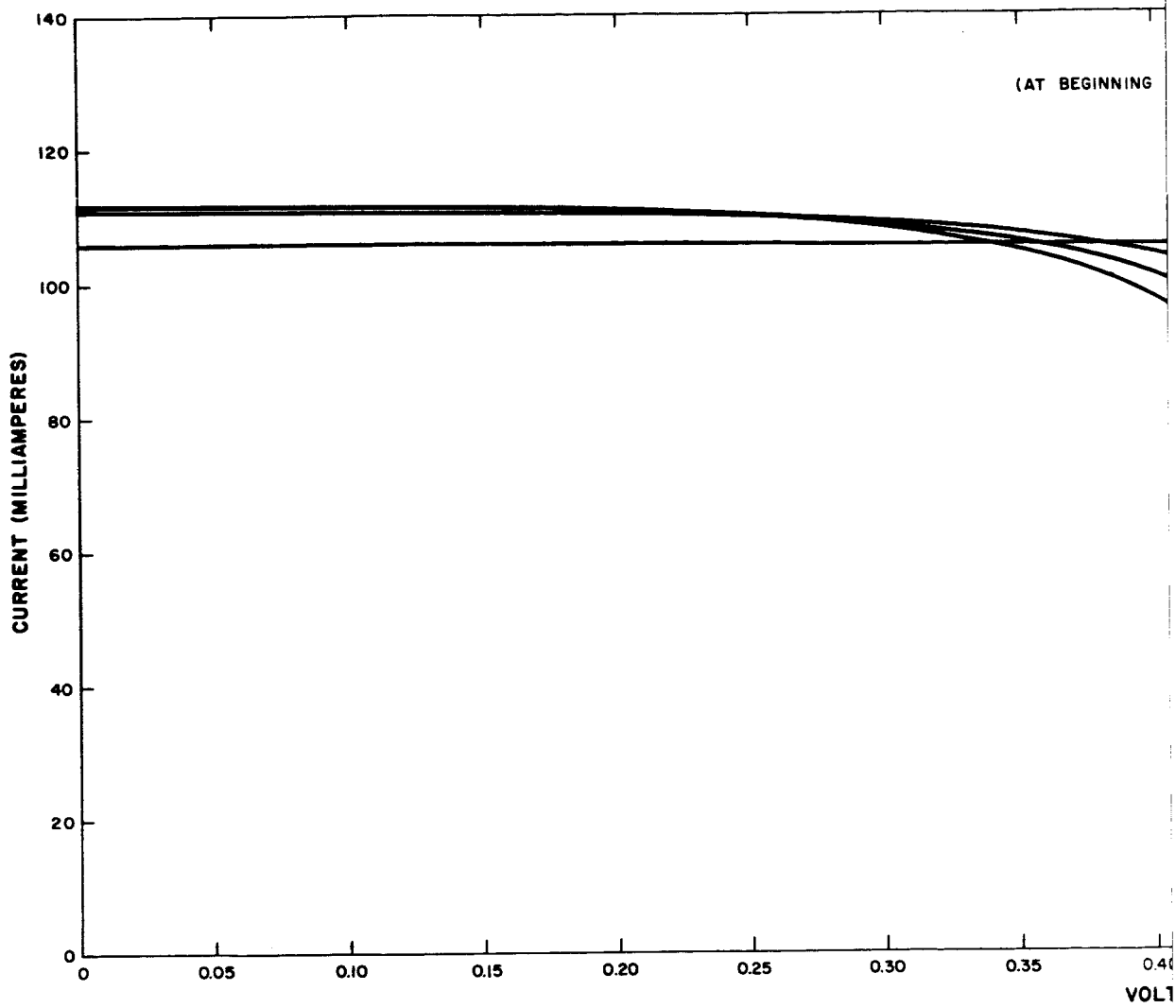
The power outputs in Table III-3 do not include allowance for random cell failures. This additional design factor shall be included in Quarterly Technical Report No. 2.

The results of the analysis in Table III-3 are then fed into an energy-balance program to determine the optimum series-parallel combination.

In addition, I-V curves for all four cases (first day design, 6 months, 9 months, and 12 months) are presented in Figures III-1 through III-4. Each figure contains four I-V curves corresponding to temperatures of -75, +25, +40 and +49 °C. For a description of the various cases, see paragraph D of this section.

TABLE III-3. SOLAR CELL/ARRAY POWER OUTPUT SUMMARY

Parameters	First Day Design	6 Months	9 Months	12 Months
Maximum Power Current of Cell in ma	101.2	88.0	85.3	82.8
Maximum Power Voltage of Cell in ma	0.405	0.4025	0.400	0.3975
Maximum Power of Cell in mw	41.0	35.4	34.1	32.9
Maximum Power of Array in watts	448.7	387.4	373.2	360
*Maximum power of cell in mw x 10,944 cells for an array.				



III-7

1

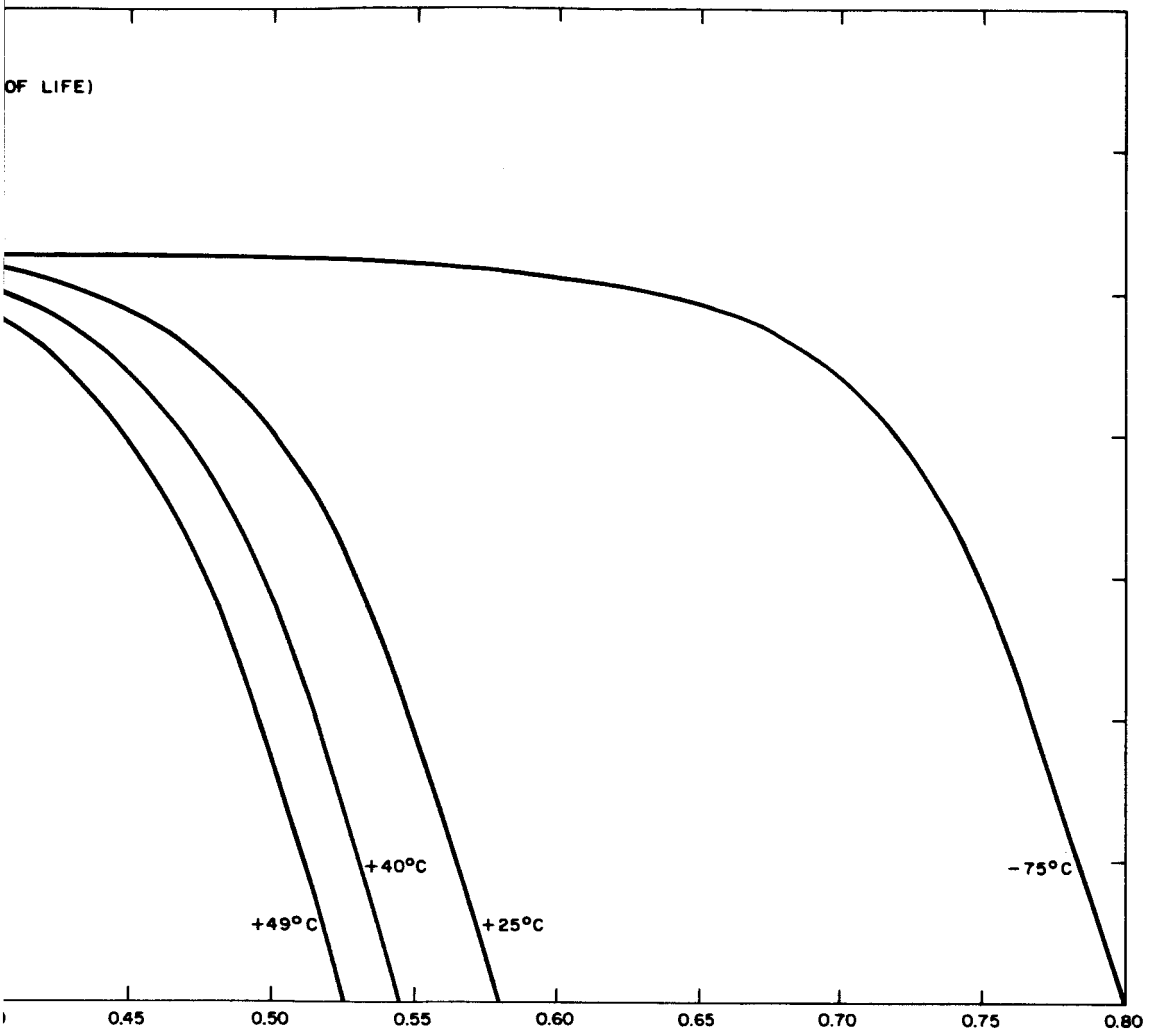
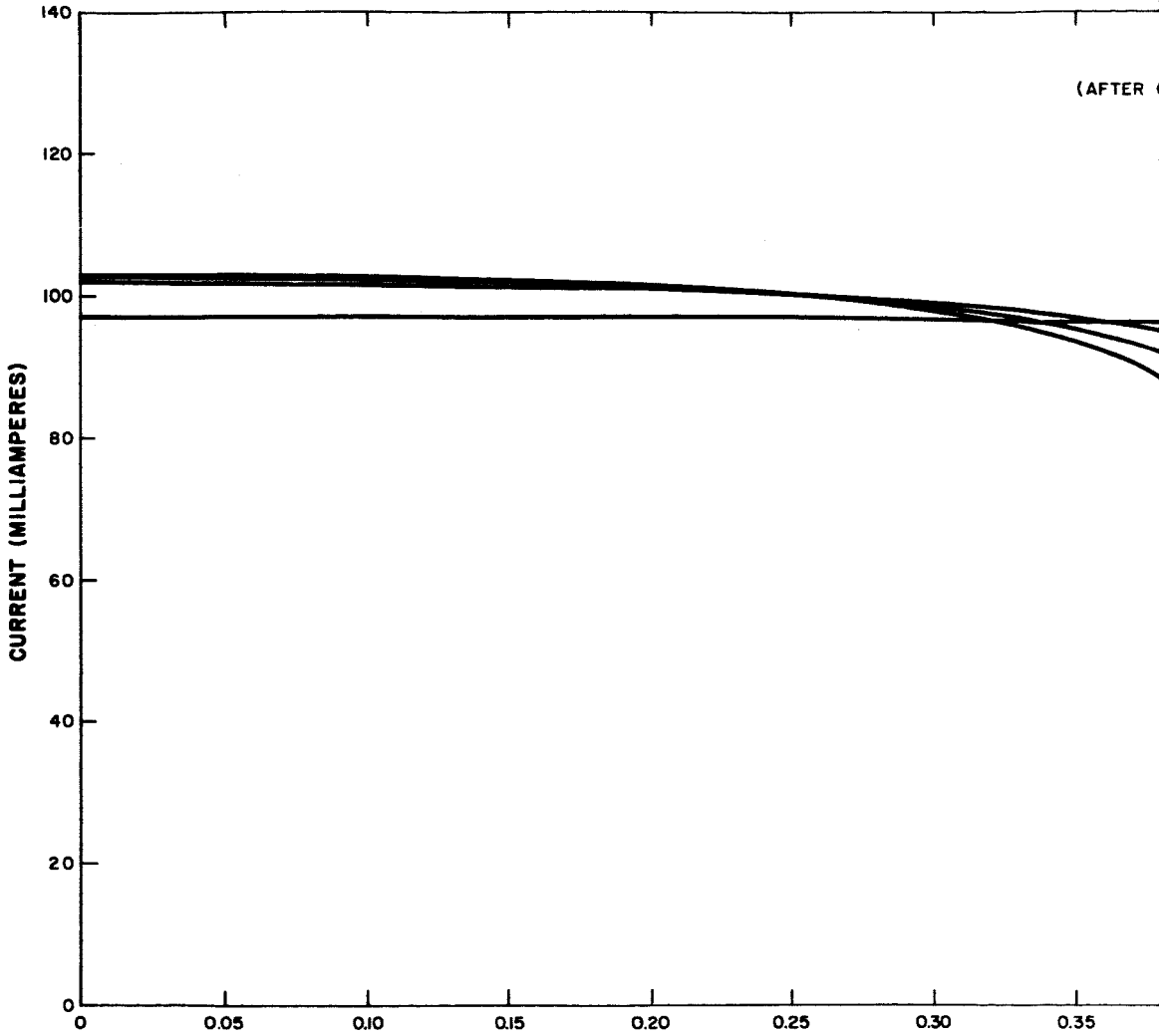
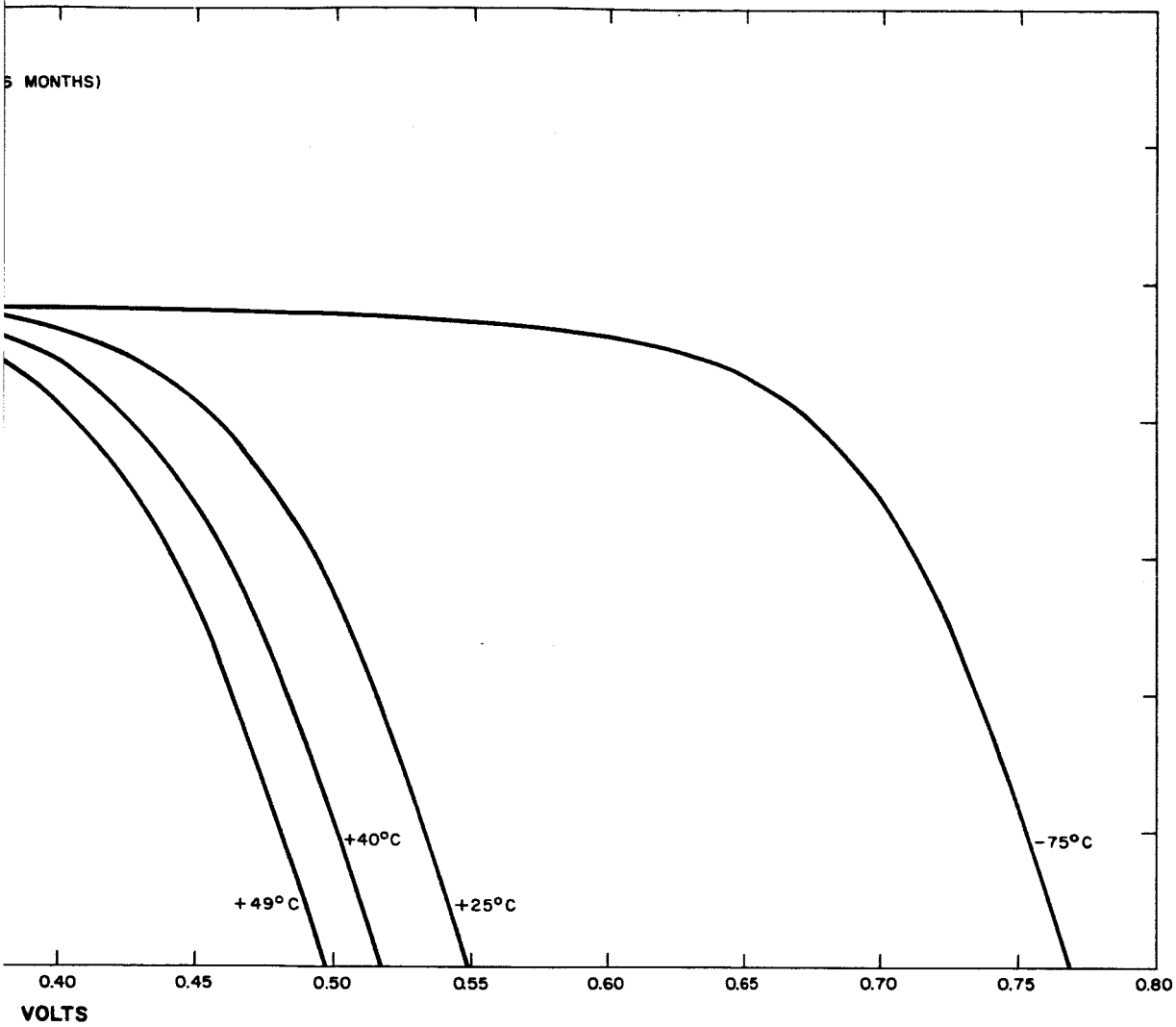


Figure III-1. Solar Cell I-V Curve
at Beginning of Life Cycle

2

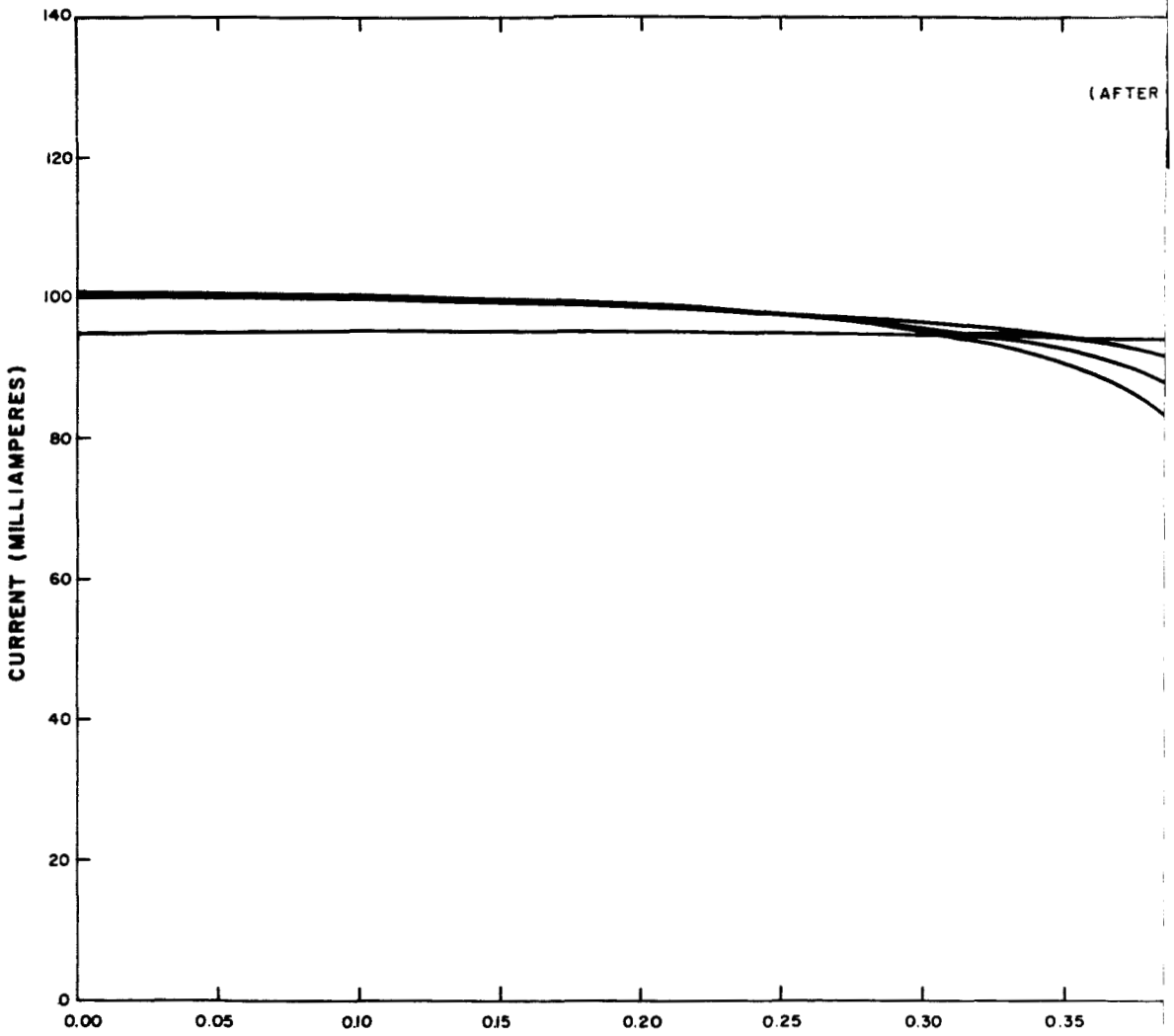


III 9

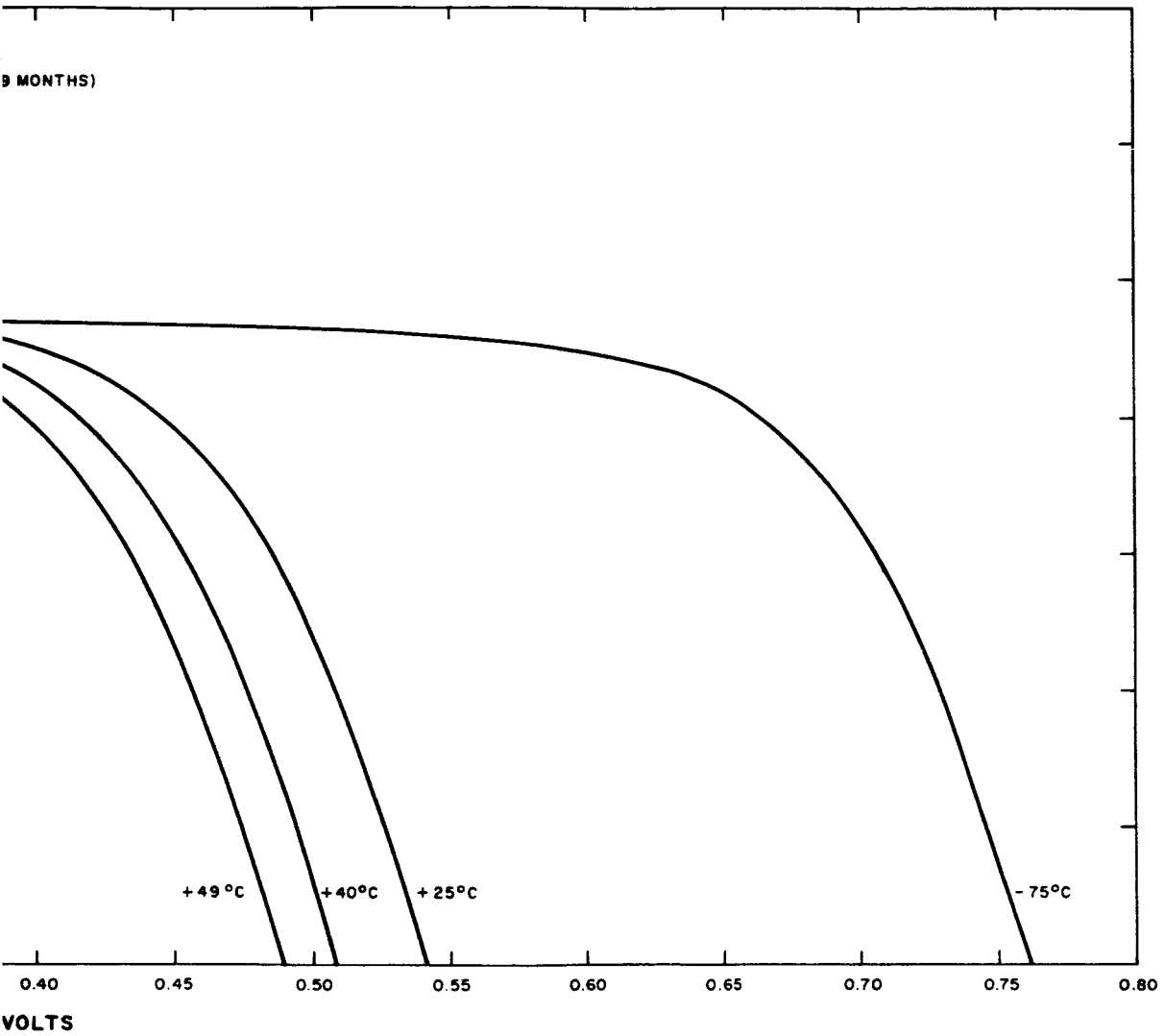


2

Figure III-2. Solar Cell I-V Curve After 6 Months of Life Cycle

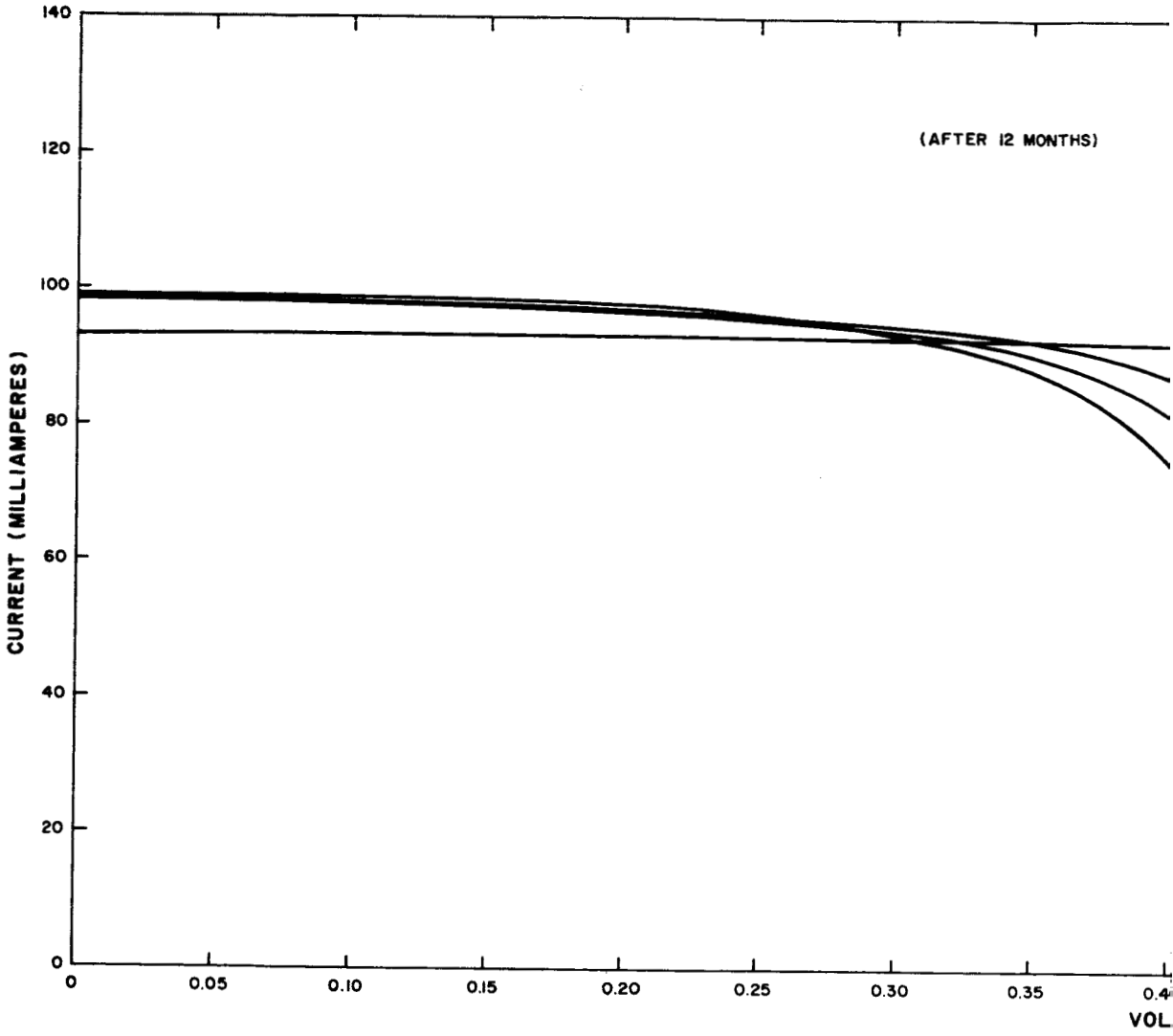


VI-11

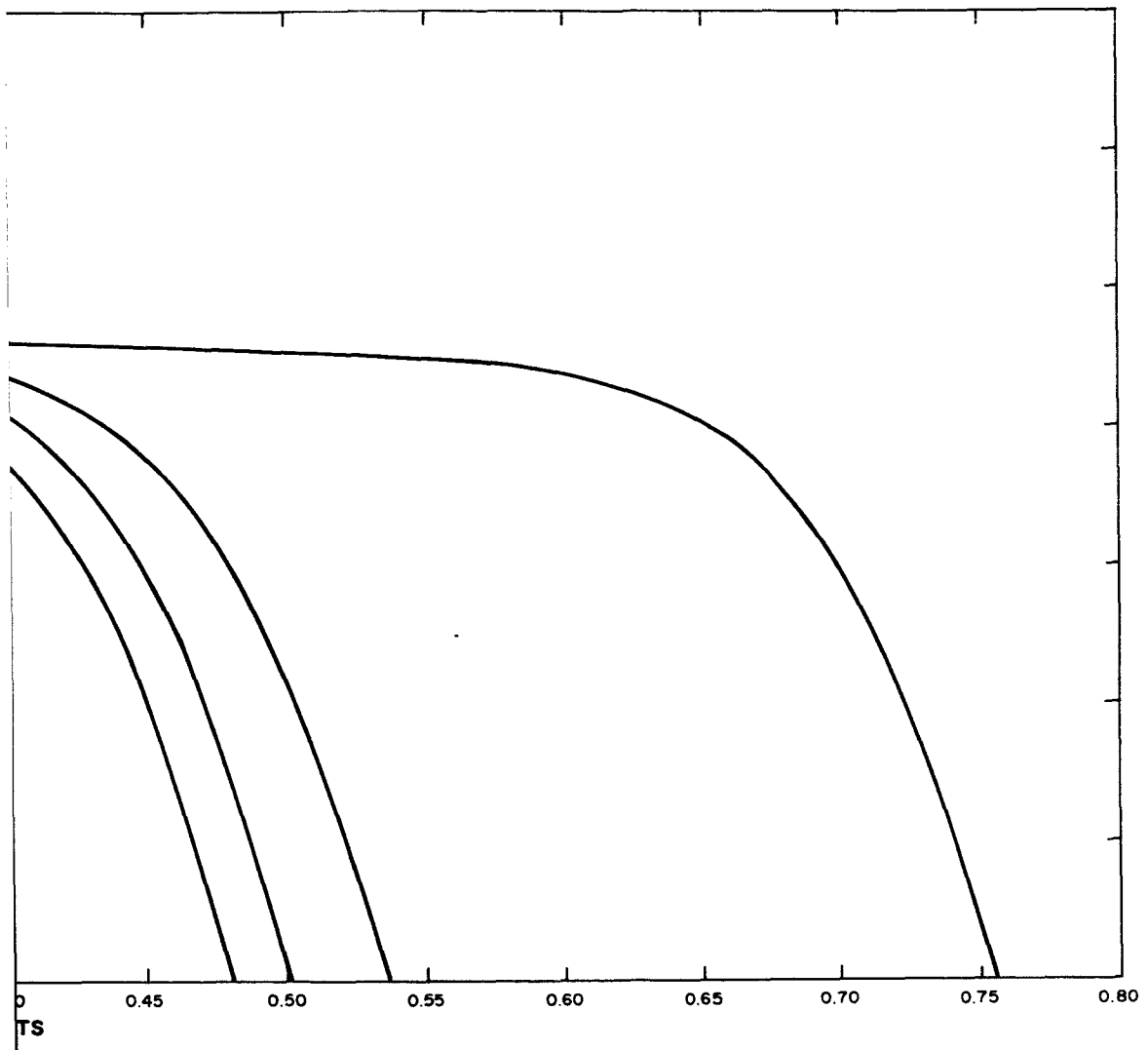


2

Figure III-3. Solar Cell I-V Curve After 9 Months of Life Cycle



III-13



2

Figure III-4. Solar Cell I-V Curve After 12 Months of Life Cycle

SECTION IV
STORAGE BATTERIES

A. GENERAL

During this report period, three main efforts were pursued in the technical study of the Nimbus-B battery module. They were:

- (1) Analysis of General Electric data on Nimbus type cells made for NASA;
- (2) Analysis of "Crane" acceptance test and cycling data for both General Electric and Gulton "Nimbus" type cells; and
- (3) Preparation of preliminary "parametric study" curves, and battery module estimated current, voltage, and heat generation.

Results and data from each of the above studies are discussed in this section.

B. ANALYSIS OF GENERAL ELECTRIC CELL DATA

AED obtained from the General Electric Company a copy of the "Acceptance Tests" data sheets titled "G. E. Process Spec. No. P24 A-PB-118, Cell Cat. No. 41B005AB01", for the 152 cells manufactured by General Electric for NASA. Figures IV-1 and IV-2 are histograms prepared from the information on these data sheets. Figure IV-1 is a set of three frequency distributions for the ampere-hour capacity of the battery cells at three different temperatures. The 25 °C capacity data used was taken from the first of the two 25 °C tests (spec. item 2.5); the second test was made following the overcharge tests, and the high capacities found are abnormal.

Table IV-1 summarizes the average ampere-hour capacity and percent standard deviation for each temperature from the set of three frequency distributions.

At 25 °C, 4.5 ampere-hour capacity is found at the minus one standard deviation or minus 6.13 percent from the average. This means that with a specification minimum of 4.5 ampere-hours, 15.9 percent of cells manufactured would be rejected. If a requirement of ± 5 percent were imposed, 41.5 percent of the cells would be rejected for the capacity requirement. The standard deviation found with the General Electric Nimbus type cells compares closely with 5.1 percent found in an analysis of 419 cells from a different cell manufacturer on a different aerospace battery program, and is considered to be the "state-of-the-art".

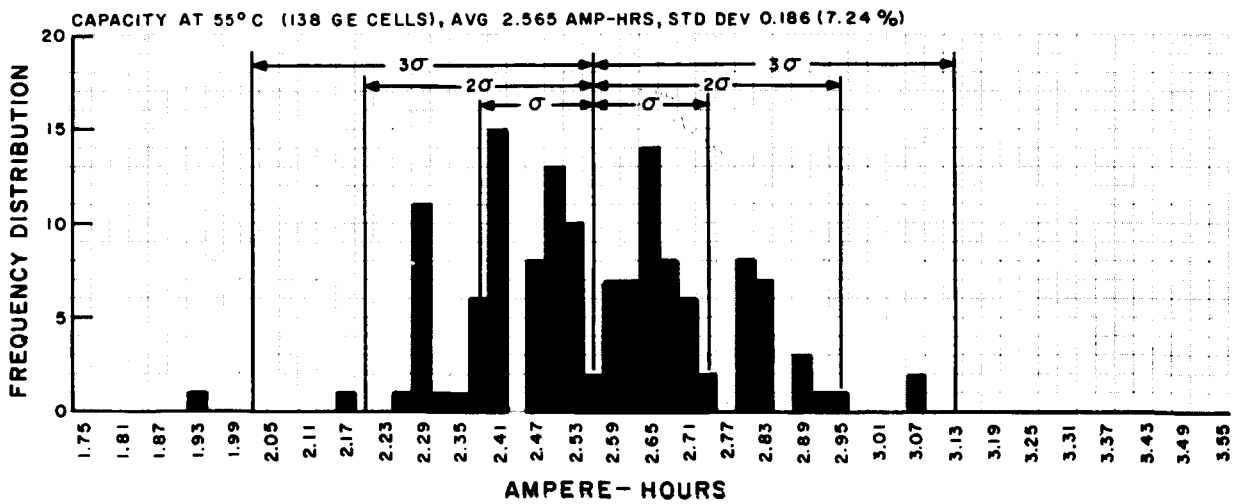
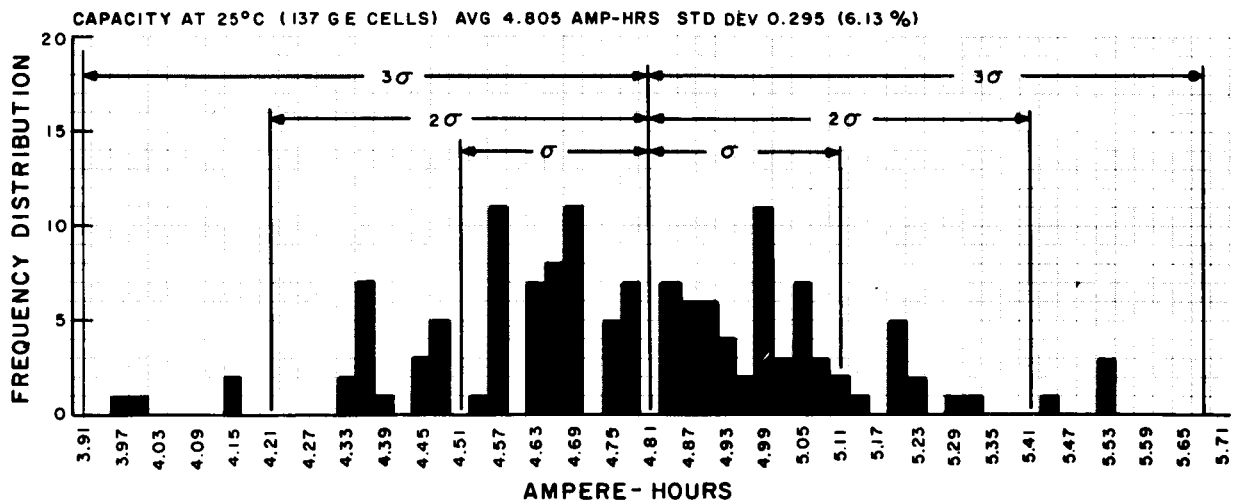
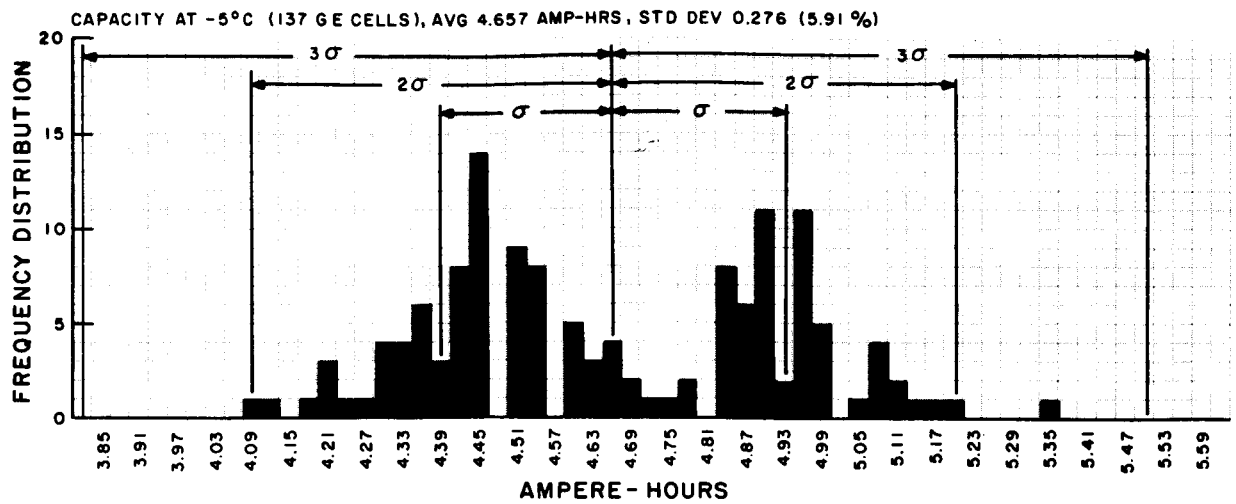


Figure IV-1. Nimbus-B Battery Cell Ampere-Hour Capacity Histograms

TABLE IV-1. SUMMARY OF BATTERY CELL FREQUENCY DISTRIBUTION DATA

Temperature °C	Avg. Capacity (Amp-Hour)	Standard Deviation (Percent)
-5	4.66	5.91
25	4.81	6.13
55	2.57	7.24

Figure IV-2 is a plot of the average cell capacity versus temperature with the maximum and minimum shown as plus and minus three standard deviations (not the actual maximum and minimum of the 137 cells tested). This figure illustrates the rapid decrease of cell capacity as temperatures exceed 30°C. The proposed temperature operating range, 10 to 30°C, is not solely based on this data, but is also based on the cycling data, and on knowledge of increasing charging difficulties at temperatures below 10°C.

C. ANALYSIS OF "CRANE" DATA

Thirty Nimbus type cells each from General Electric and Gulton Industries were submitted to the Quality Evaluation Laboratory of the U.S. Naval Ammunition Depot at Crane, Indiana by NASA. These cells were subjected to an "Acceptance Test" program (which was reported in two published test reports: QE/C 65-459 for the General Electric cells, and QE/C 65-460 for the Gulton cells), and a "cycling" program which was not completed, but from which data was supplied to AED by NASA.

Figure IV-3 shows the frequency distributions of cell capacities taken from the two Acceptance Test reports. The data in each case is for the last of the three capacity tests performed on the cells. In the conclusions and discussion of capacity in the Acceptance Test reports, the first capacity test was evaluated. This first test immediately followed the conditioning procedure, and like the General Electric data of capacity immediately following the overcharge test, it is abnormally high. In most battery test procedures, the results of the last of three capacity tests are accepted as the realistic capacity, since the affect of previous cell history has been eliminated and is generally presented as a reproducible figure.

The data in the Acceptance Test reports are of limited value due to the absence of cell temperature information. This is particularly true for the overcharge voltages where, in some cases, it appears that the cell temperature must have departed radically from the ambient temperature and the data is inconsistent.

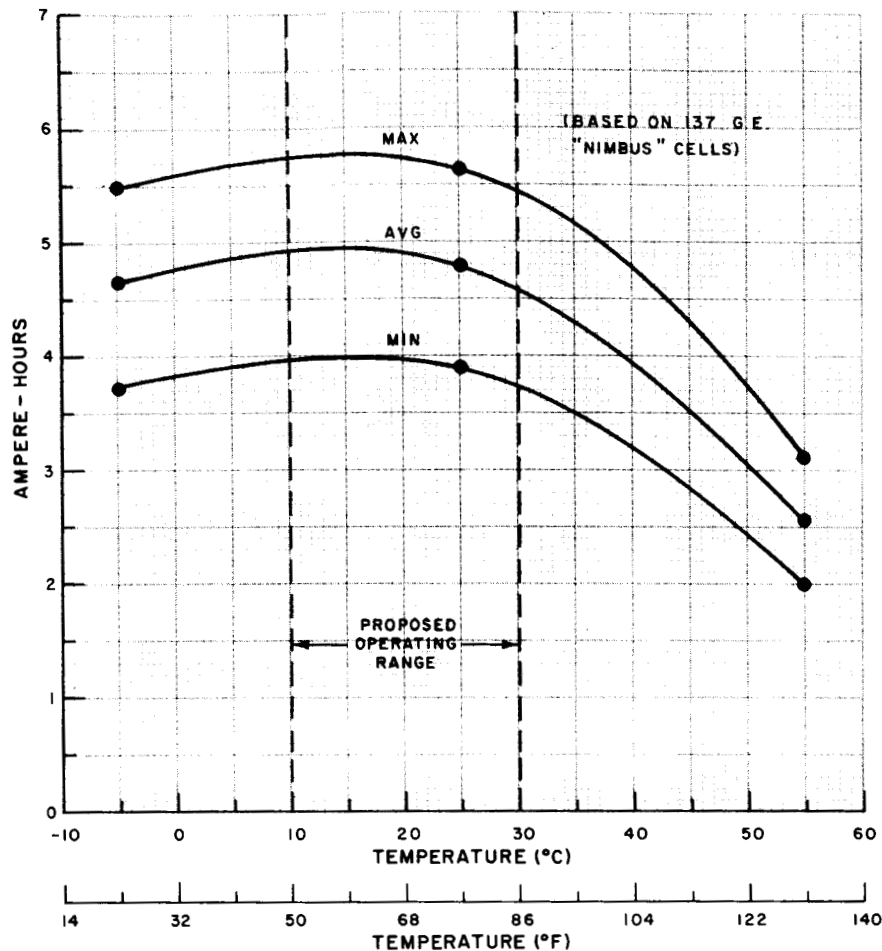


Figure IV-2. Average Cell Capacity (Ampere-Hours) Versus Temperature

The "Crane" cycling tests consist of testing six groups of five cells from each cell manufacturer at three temperatures (0°C, 25°C, and 40°C) and two depths of discharge. The data have been made available to AED for the first 1800 cycles for the 15 percent depth of discharge tests, and the first 1200 cycles for the 25 percent depth of discharge tests. These data are plotted on Figure IV-4 for the General Electric cells and on Figure IV-5 for the Gulton cells; both end-of-charge and end-of-discharge voltages are plotted as a function of cycle number.

The data from Figures IV-4 and IV-5 have been cross-plotted on Figures IV-6, IV-7, and IV-8, to show the average cell voltage at end-of-discharge both as functions of depth of discharge and of temperature, for four selected time cycles: 250 cycles, 750 cycles, 1250 cycles, and 1750 cycles, respectively. Figure IV-9 shows the average cell voltage at end-of-discharge as a function of temperature only. (The depth of discharge data were not available at this time.) The voltages for the Gulton cells can be observed to be more sensitive to increasing depth of discharge or increasing temperature; but for

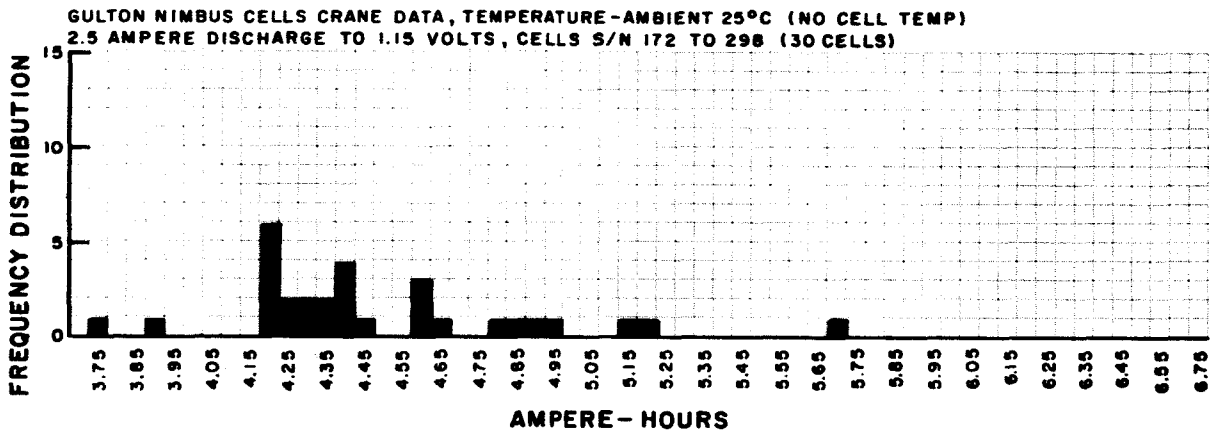
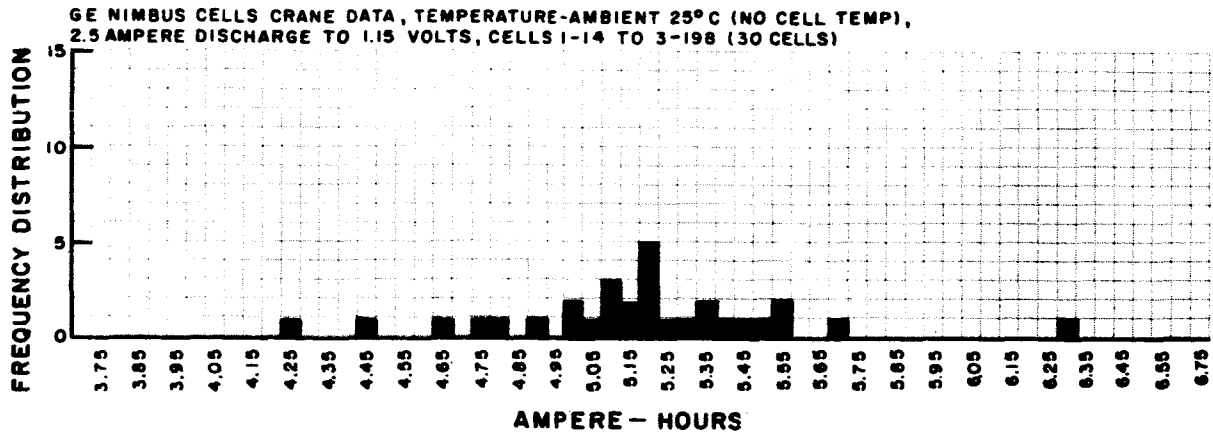


Figure IV-3. Cell Capacity Frequency Distribution Histograms

both General Electric and Gulton cells, it can be observed that the end-of-discharge voltage decreases radically above 30°C.

Figures IV-10 and IV-11 show a plot of average end-of-discharge voltage for 15 percent and 20 percent depth of discharge for 10°C and 30°C. These parameters were selected as most nearly representing the Nimbus-B mission load requirements, and a temperature range that makes a one-year cycling program feasible. (The points plotted in Figures IV-10 and IV-11 were obtained from Figures IV-6, IV-7, IV-8, and IV-9.) With the data available, it is not yet possible to predict the results of one year of cycling with any confidence.

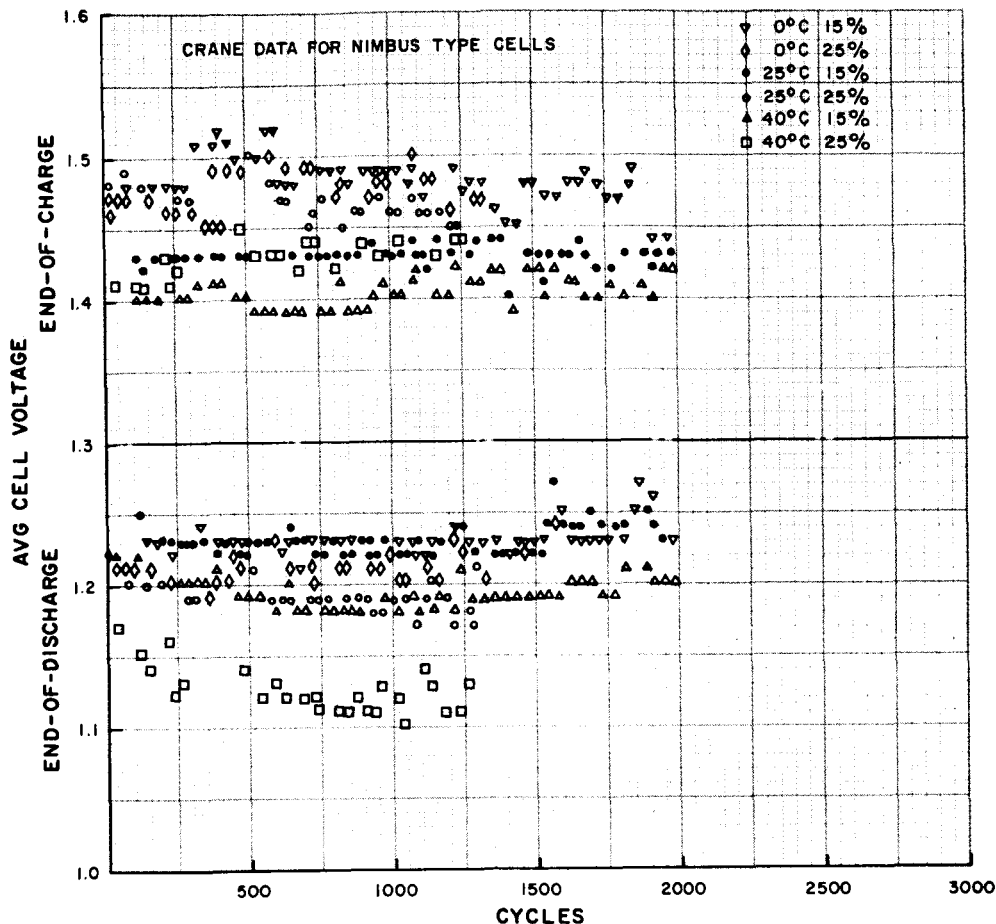


Figure IV-4. General Electric Average Cell Voltage Versus Cycle

D. PRELIMINARY "PARAMETRIC STUDY CURVES" AND BATTERY MODULE ESTIMATED CURRENT, VOLTAGE, AND HEAT GENERATION

In order to proceed with the computer program for the Nimbus-B power supply subsystem, it was necessary to provide data as computer inputs. Estimates were made of cell discharge and charge voltages at 25°C for various discharge and charge currents as a function of time; this was plotted in Figure IV-12. Additional data was also required to estimate the effect of continuous cycling on these discharge and charge voltages, and estimates were made for data reflecting 6 months, 9 months, and 12 months of continuous cycling. These estimates were plotted in Figures IV-13, IV-14, and IV-15.

Since no actual cycling program simulating the Nimbus-B mission has been completed, the estimates for 6, 9, and 12 months are subject to considerable revision when more data becomes available.

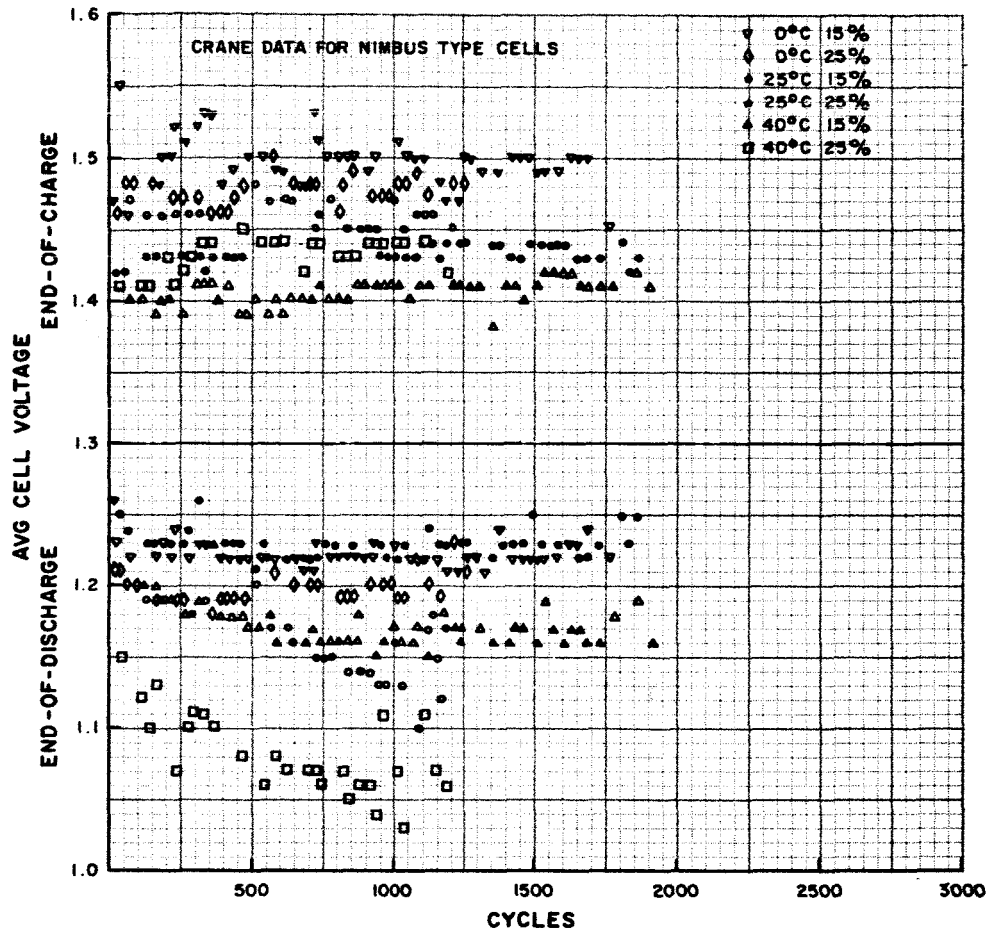


Figure IV-5. Gulton Average Cell Voltage Versus Cycle

Figure IV-16 is a set of curves showing the estimated battery module current voltage and heat generation versus time for one orbit. These curves are specifically for 25°C, and the current values are estimates based on experience with nickel-cadmium cells other than the Nimbus cells. No attempt was made to include an affect due to extended cycling.

The heat generation curve shown in Figure IV-16 is based on an energy balance. All electrical energy input to the nickel-cadmium cells in excess of the energy withdrawn during discharge is shown as heat generation. Although it is known that there is some heat absorption during the normal charge period, this is not shown, since it is estimated to be of a magnitude that would cause little change in the distribution of the overall heat generation, and would not change the total heat generation. Although the heat generation curve shown was calculated based on theory, it has been found in the past that such a curve approximates closely the results of actual laboratory tests in a calorimeter. This heat generation is limited to the heat generated within the nickel-cadmium cells, and in no way includes heat generated in electronic equipment associated with the battery module.

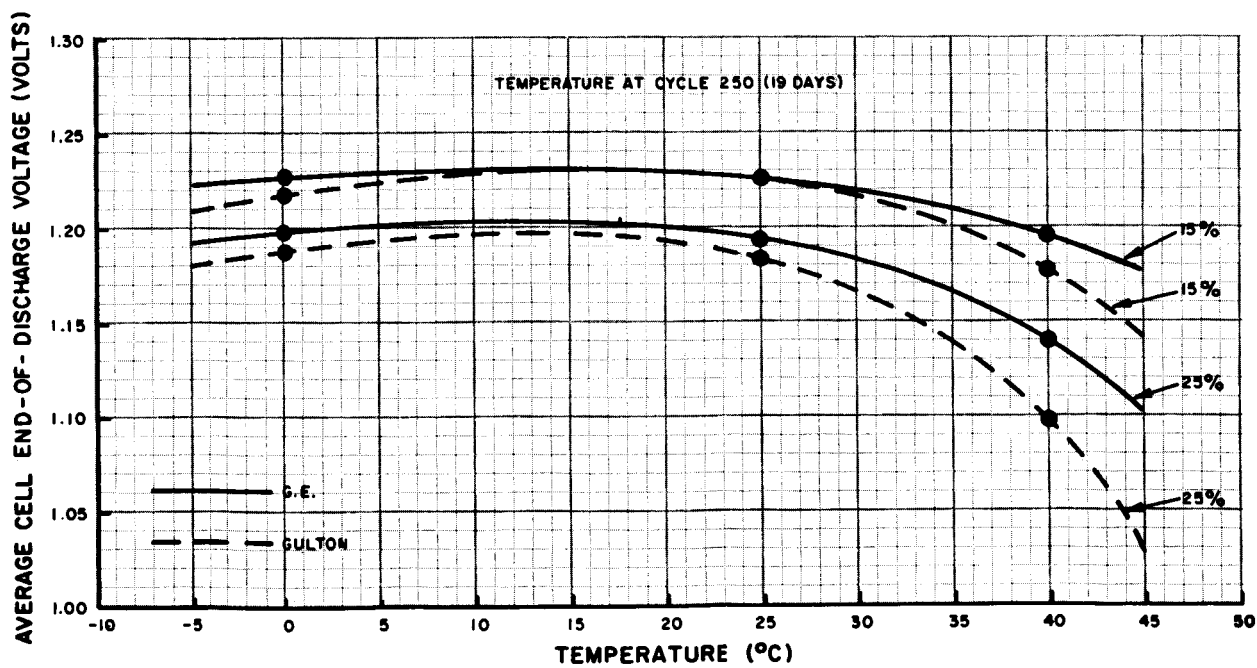
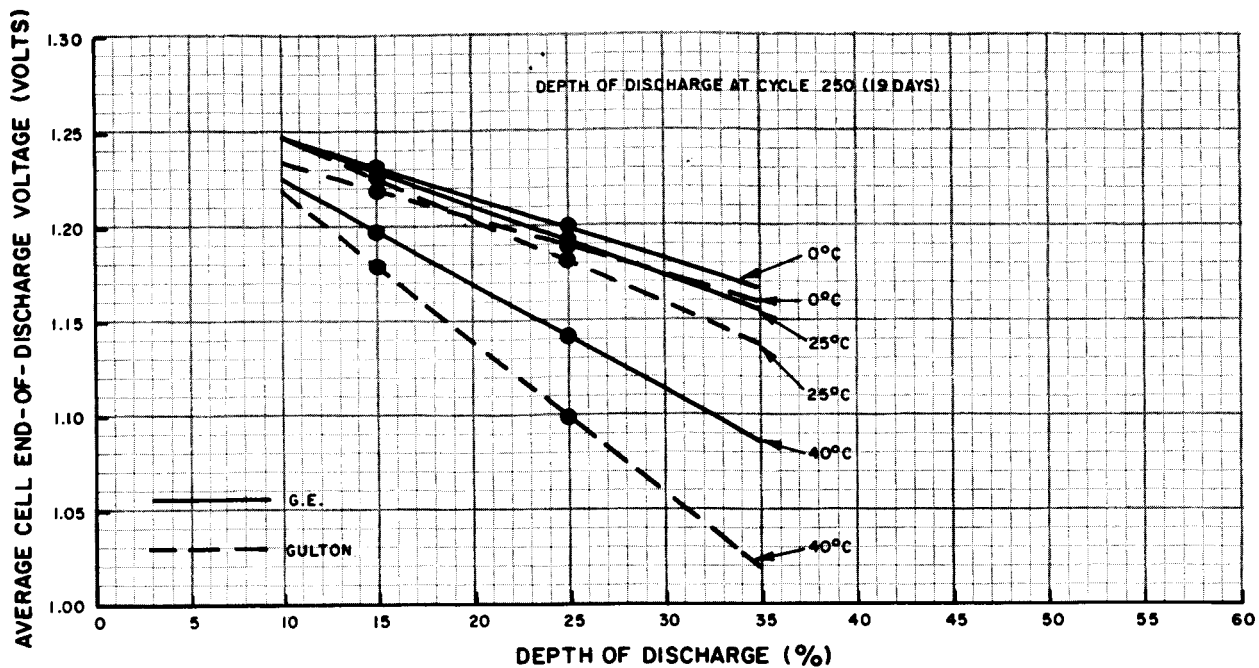


Figure IV-6. Average Cell Voltage Versus Depth of Discharge and Temperature at 250 Cycles

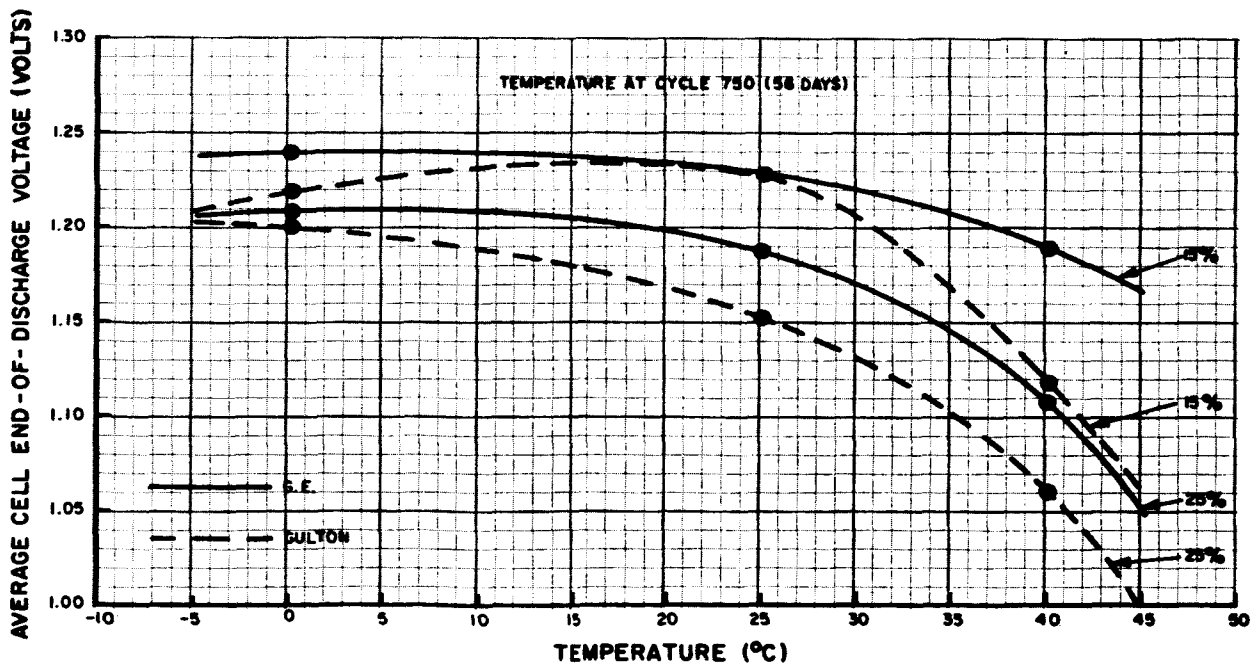
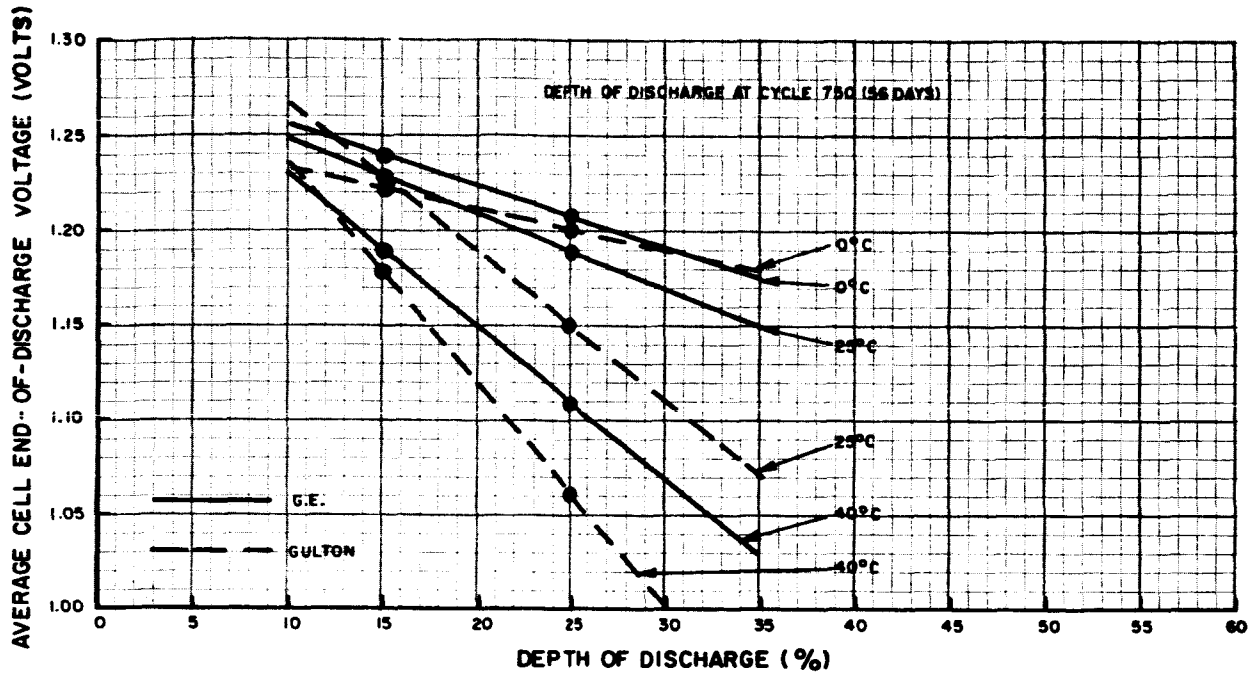


Figure IV-7. Average Cell Voltage Versus Depth of Discharge and Temperature at 750 Cycles

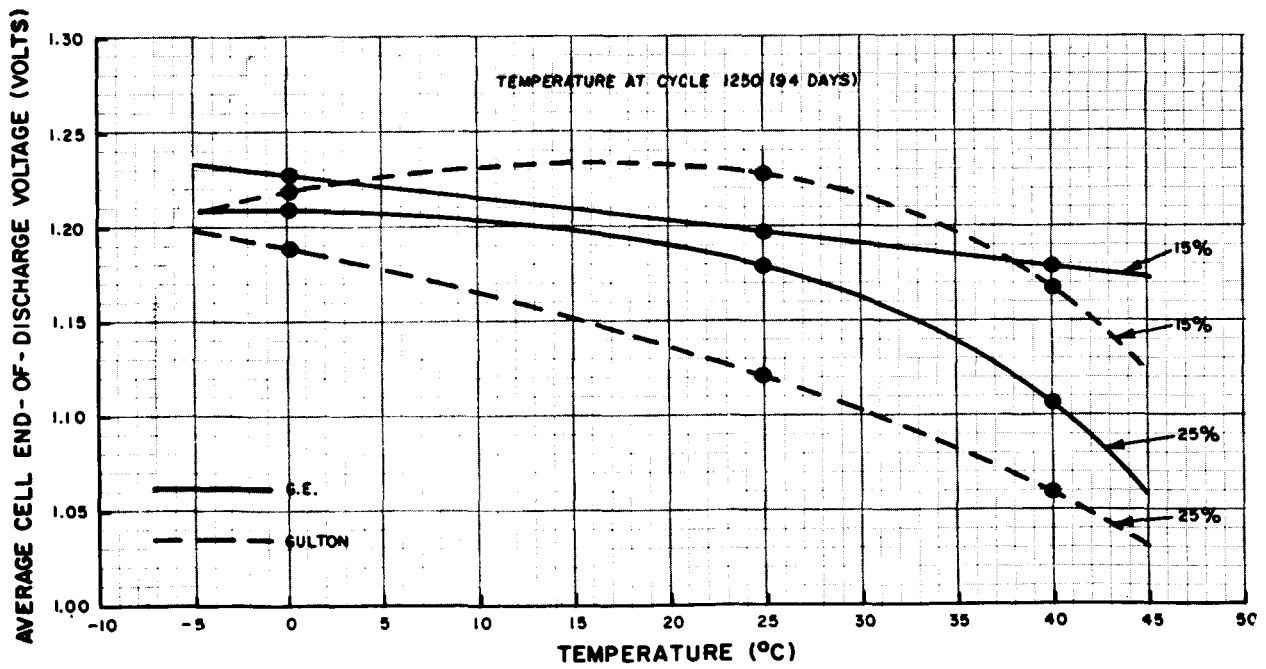
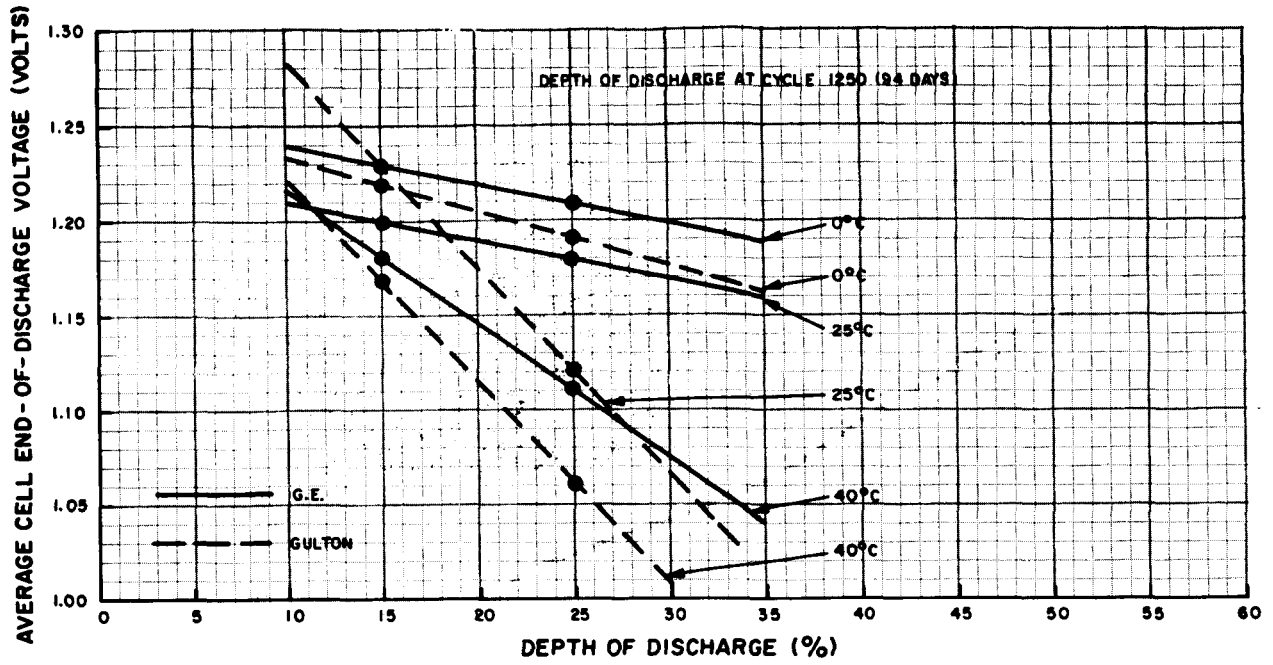


Figure IV-8. Average Cell Voltage Versus Depth of Discharge and Temperature at 1250 Cycles

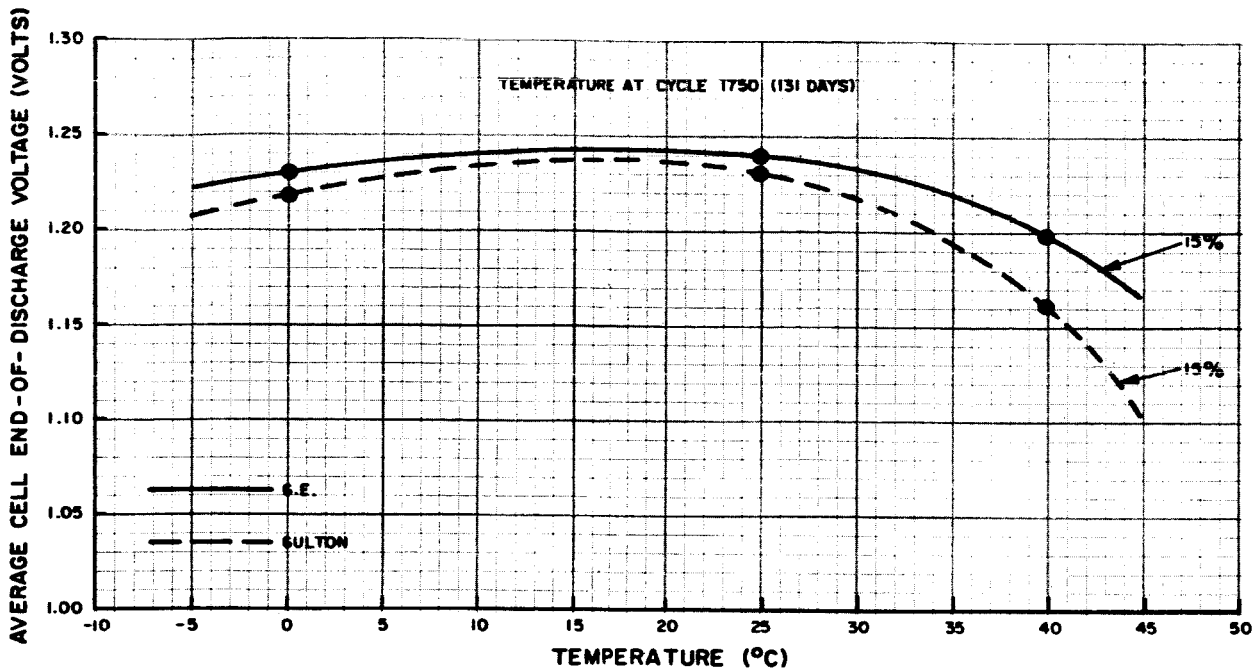


Figure IV-9. Average Cell Voltage Versus Depth of Discharge and Temperature at 1750 Cycles

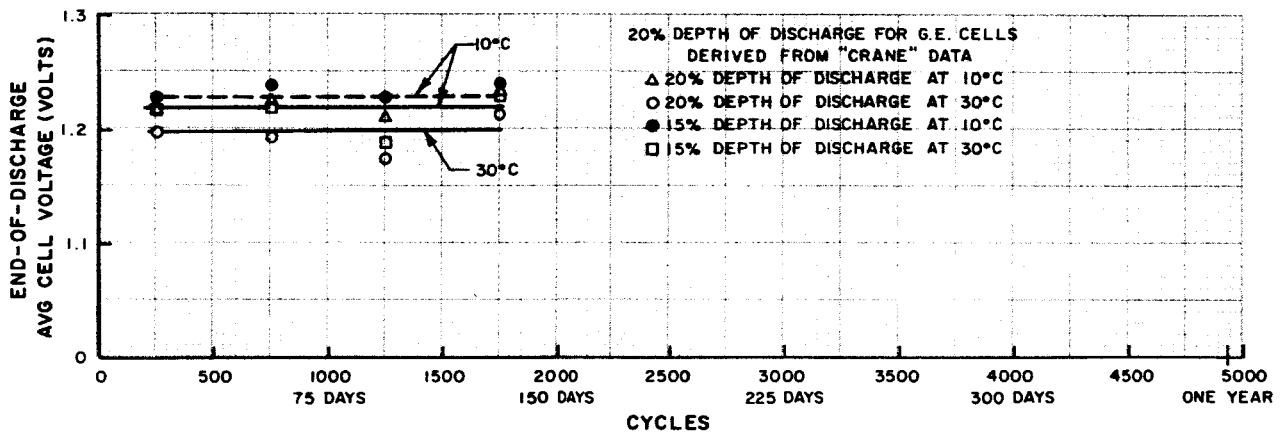


Figure IV-10. Average Cell Voltage Versus Cycle at 20 Percent Depth of Discharge for General Electric Cells

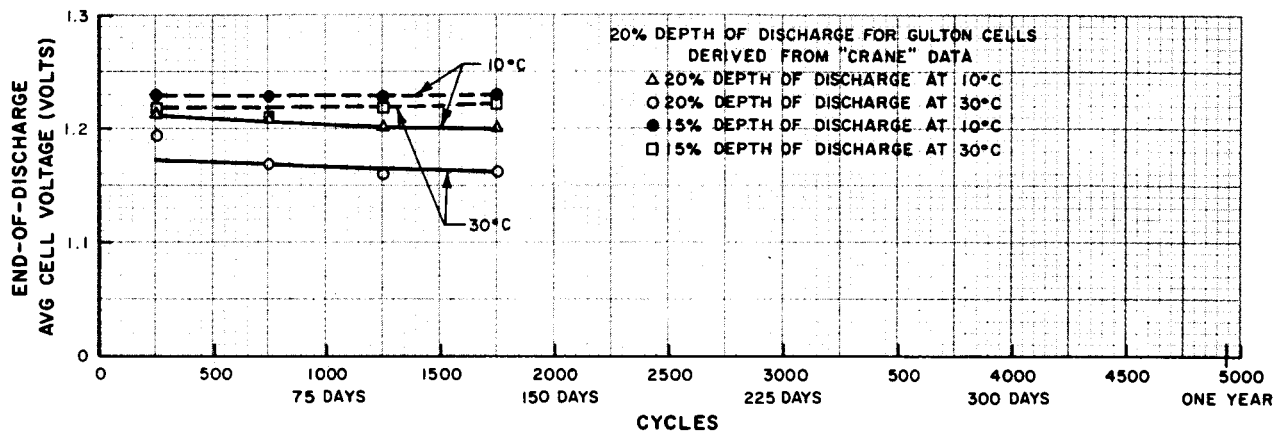


Figure IV-11. Average Cell Voltage Versus Cycle at 20 Percent Depth of Discharge for Gulton Cells

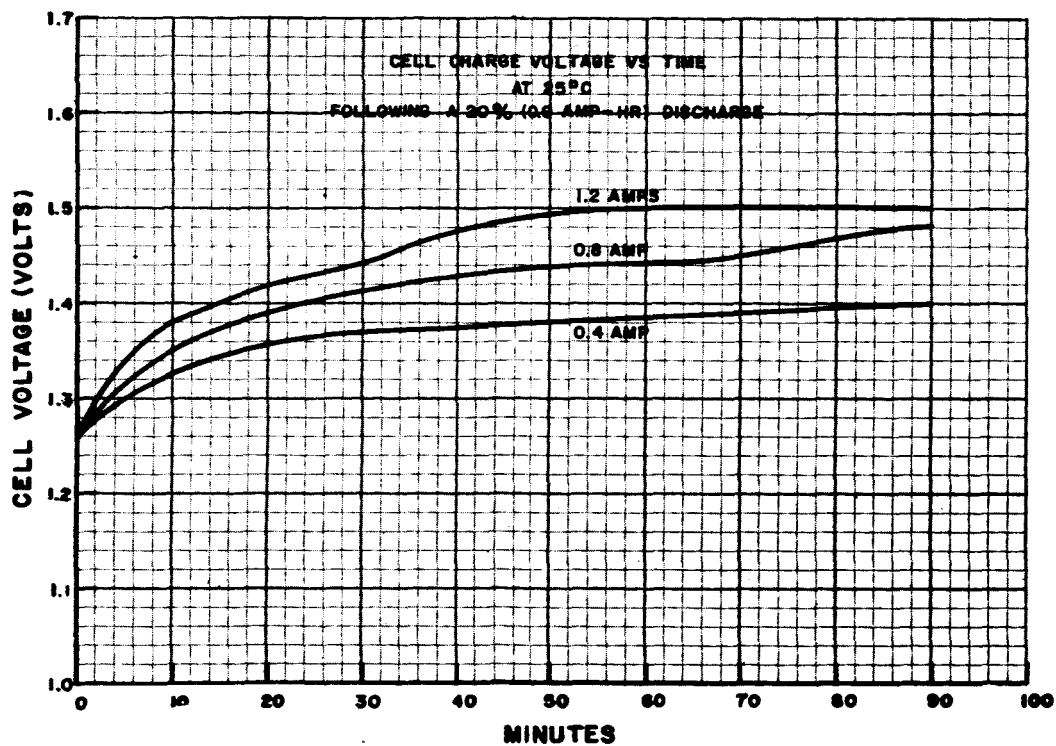
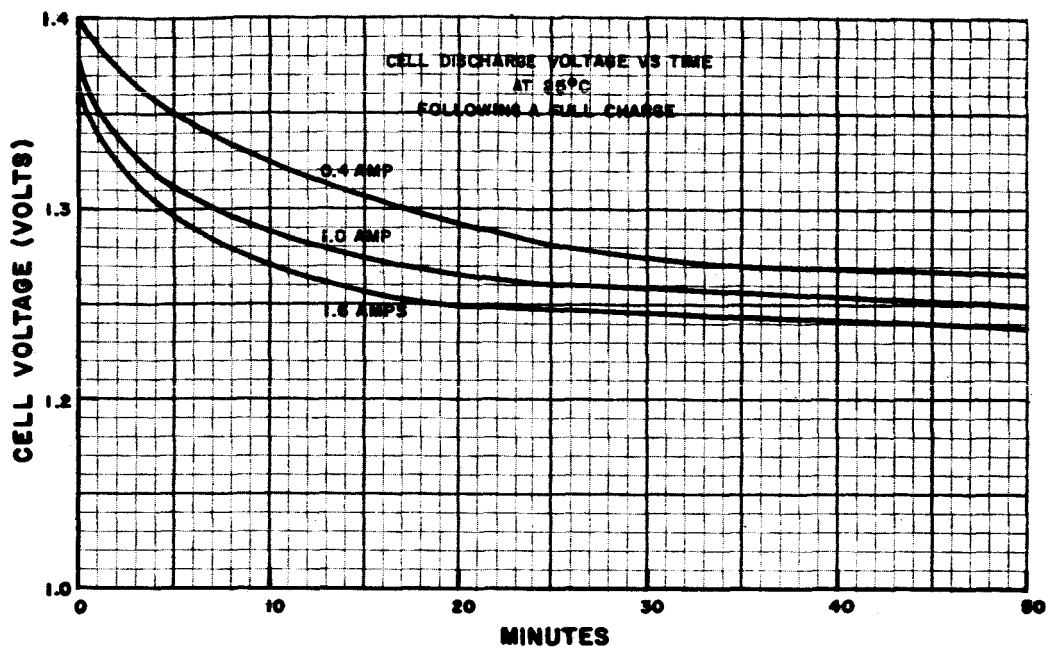


Figure IV-12. Cell Charge and Discharge Voltages Versus Time at 25°C

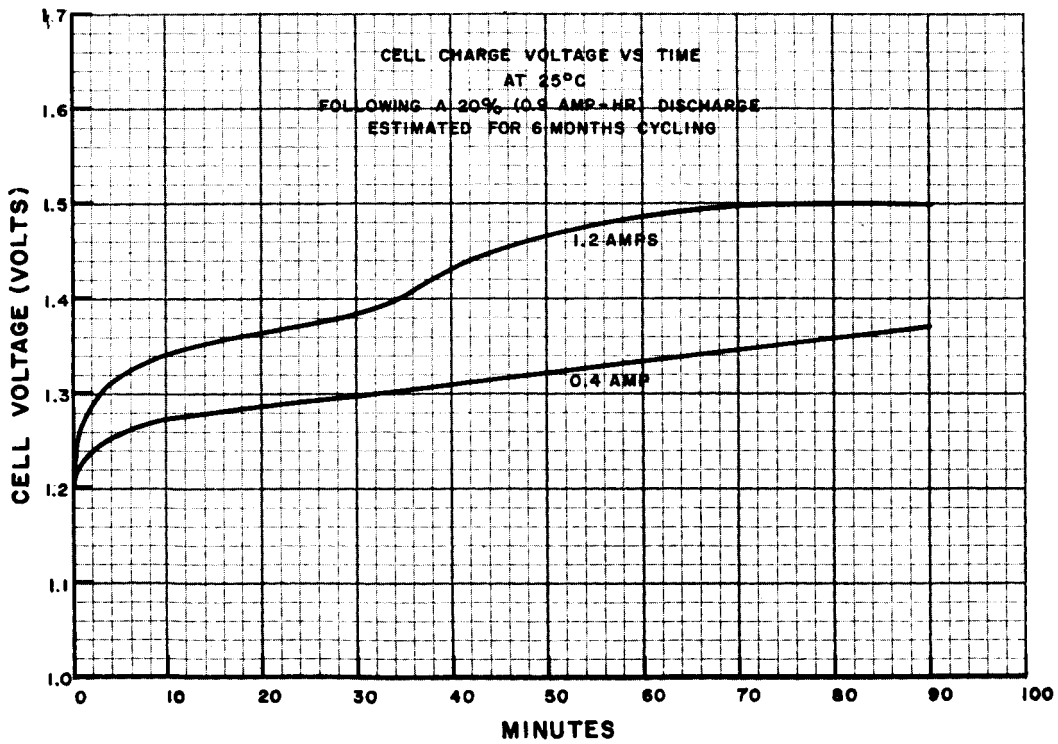
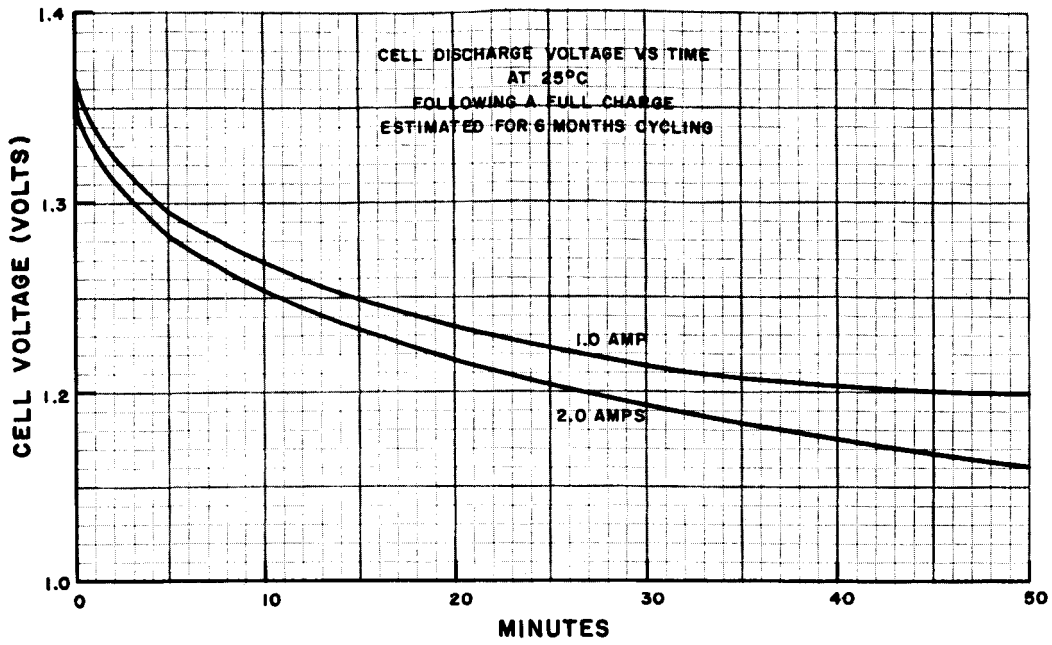


Figure IV-13. Cell Charge and Discharge Voltages Versus Time at 25°C for 6 Months Cycling

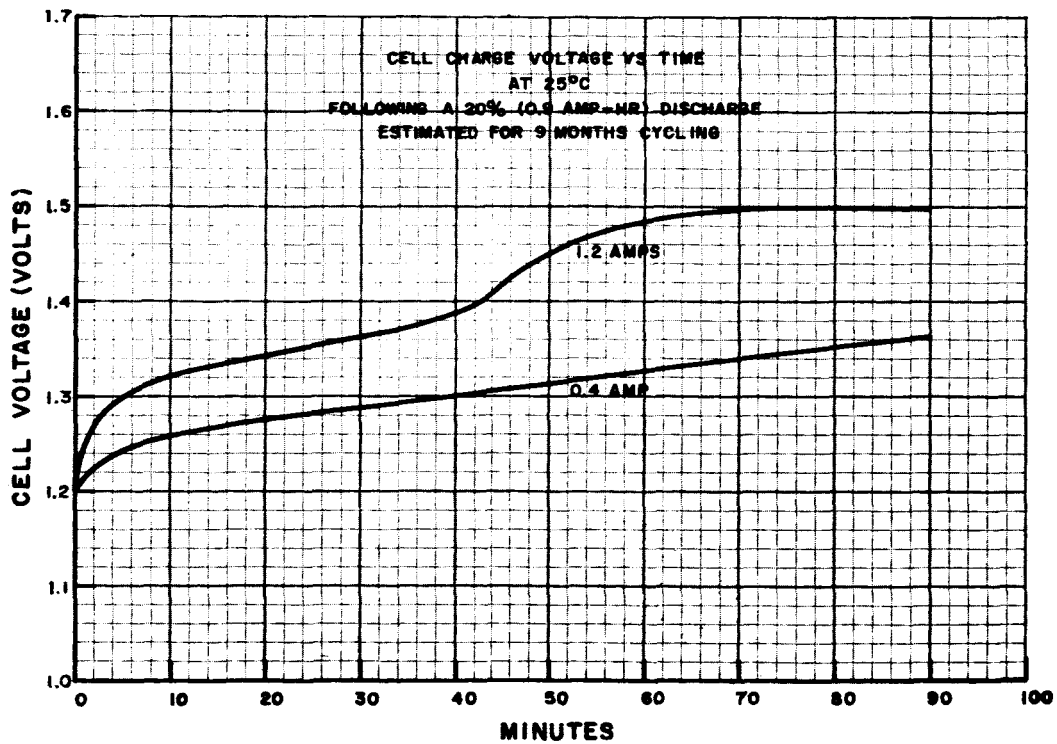
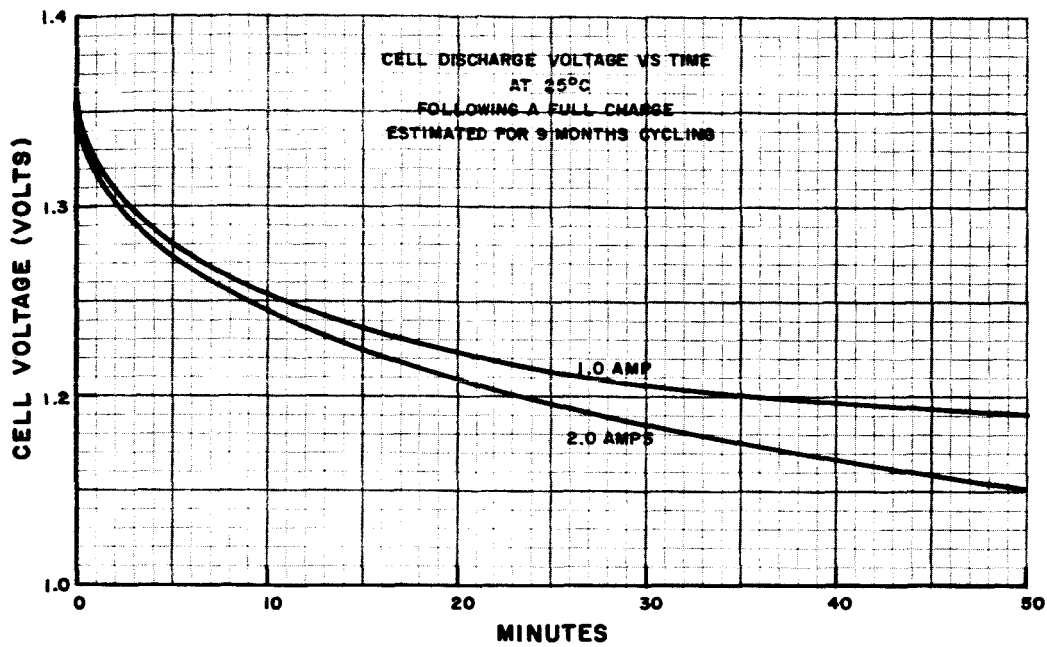


Figure IV-14. Cell Charge and Discharge Voltages Versus Time at 25°C for 9 Months Cycling

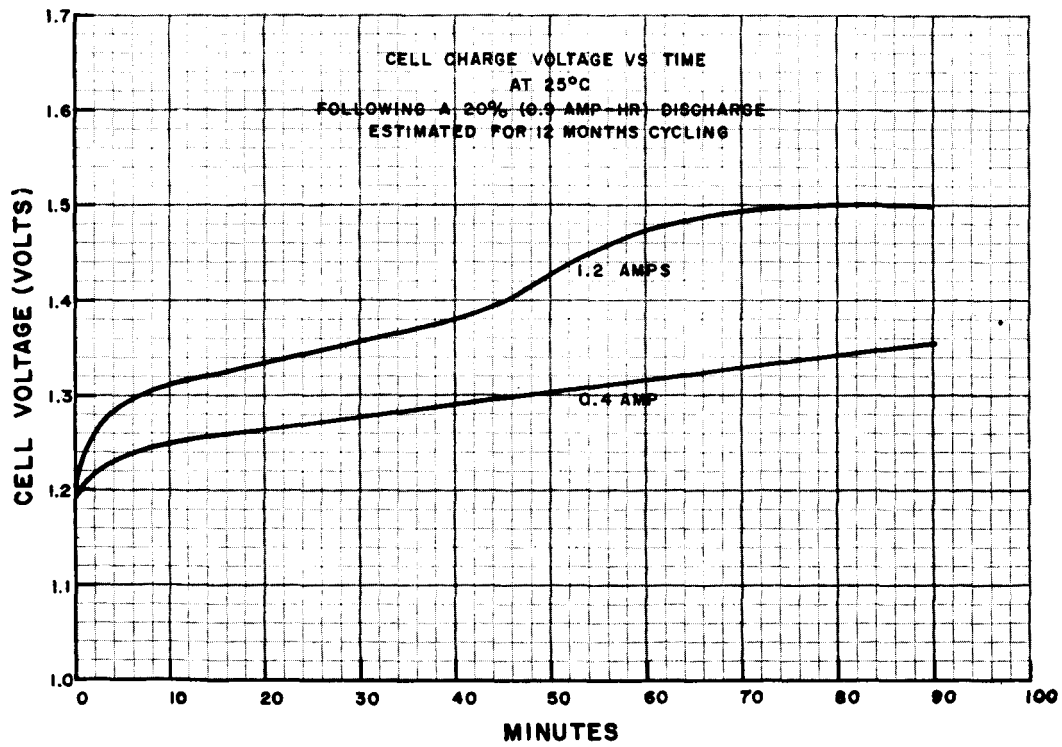
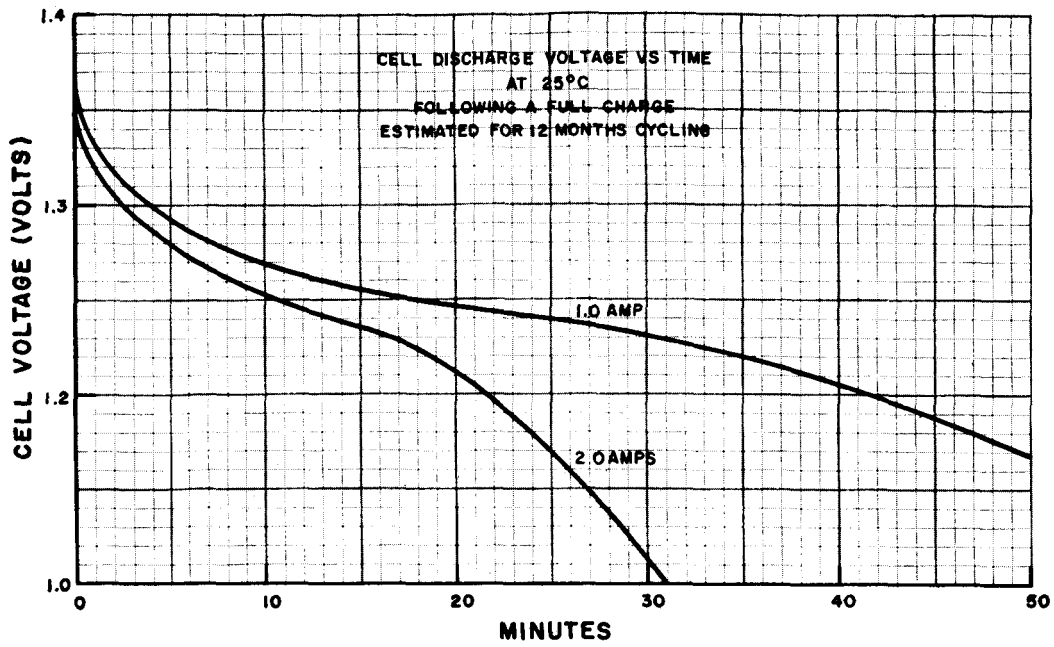


Figure IV-15. Cell Charge and Discharge Voltages Versus Time at 25°C for 12 Months Cycling

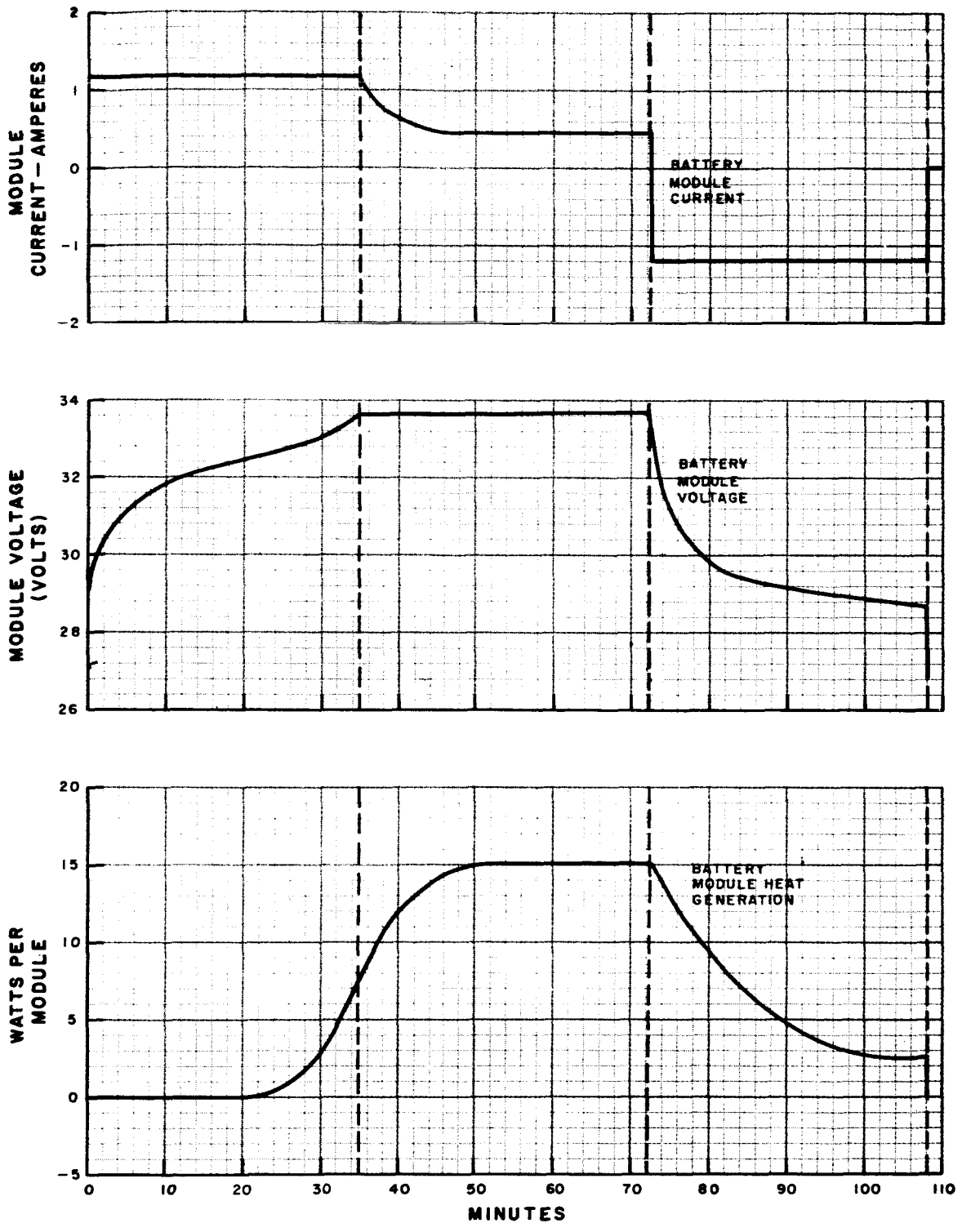


Figure IV-16. Battery Module Estimated Current, Voltage, and Heat Generations Versus Time at 25 °C



SECTION V

BATTERY CONTROL AND PROTECTION CIRCUITS

A. GENERAL

The electronics of the Nimbus-B battery module are being developed to serve three major purposes. Its primary function is to control the recharging of the Ni-Cd battery contained in the battery module. The second purpose is to provide analog signals proportional to battery parameters for the spacecraft telemetry subsystem. The third function of the battery electronics is to provide a means whereby certain ground commands received via the spacecraft telemetry subsystem may be executed.

The battery module also contains a transistor which is part of one of the heat-dissipating legs for the spacecraft shunt limiter. Although this circuit bears no direct relationship to battery operation, the battery module provides a convenient location in the spacecraft from which the heat developed by the transistor may be dissipated.

A functional block diagram of the Nimbus-B battery module is shown in Figure II-3.

B. BATTERY CHARGE CONTROL

1. GENERAL

The purpose of the battery charge controller is to protect the battery from over-current, over-voltage, and over-temperature conditions while it is being charged.

The control circuitry performs this function by monitoring and operating upon the following parameters:

- (1) Battery charge current,
- (2) Battery temperature, and
- (3) Battery terminal voltage.

The control circuitry will be designed to accept signal inputs corresponding to each of the above parameters and to compare these inputs with built-in references. Deviations or error signals will be amplified and will ultimately adjust battery charging current in such a manner as to decrease the error.

There are three normal modes in which the charge controller might operate. These modes or regions of operation are indicated in Figure V-1.

2. REGION I OPERATION

In Region I, it is desired to maintain charging current as close as possible to the maximum allowable current. In addition, any current less than that required to maintain energy balance could result in a mission failure through insufficient charging. The tolerance requirements on the charge current have dictated a closed loop or feedback type of current regulating circuit.

Figure V-2 presents a block diagram of the current regulator. In Figure V-2, the symbol, V_{R1} , represents a reference voltage derived from a temperature compensating zener diode and a voltage divider. The symbol " G_1 " represents the forward gain or transconductance of the transistor circuitry; " h " represents the feedback element which senses battery current, I_B , and transforms the current level to a voltage level which is compared with V_{R1} . The difference between V_{R1} and the converted current level is the error, E , which activates the forward gain to control the charge current.

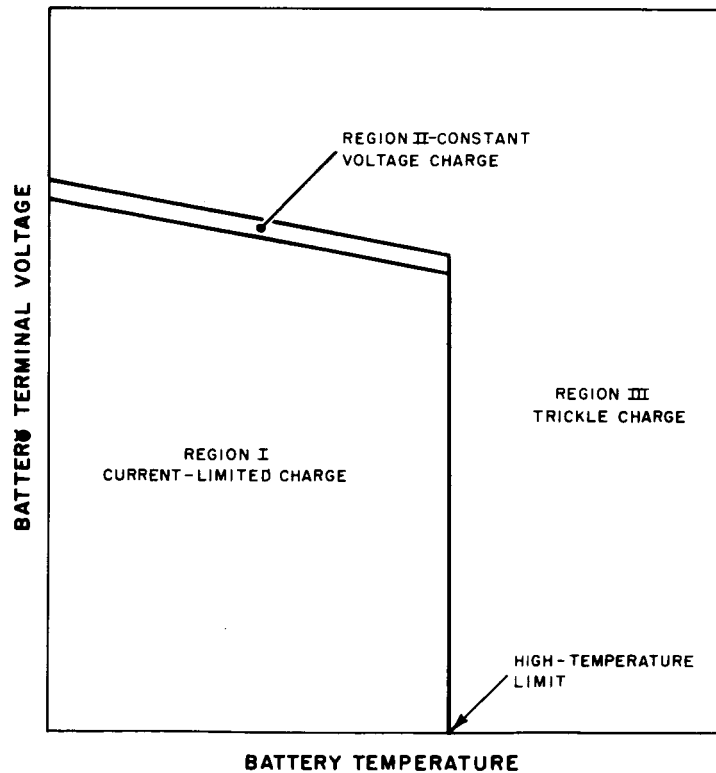


Figure V-1. Regions of Normal Charge Controller Operation

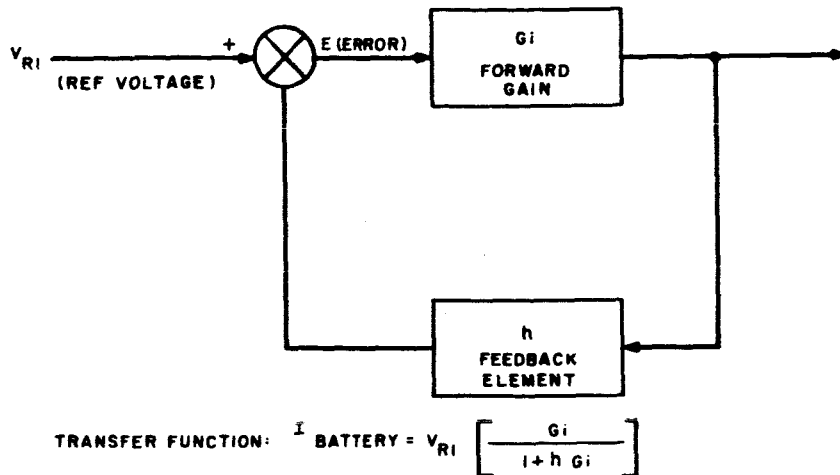


Figure V-2. Current Regulator Block Diagram

3. REGION II OPERATION

In Region II, it is desired to limit the voltage to which the battery may charge. It is also desired to adjust this limiting voltage with battery temperature in the manner suggested in Figure V-3.

Normally, at the beginning of charge, the battery will cause the charge controller to operate in Region I, the current limited mode. As the battery is charged, either or both its terminal voltage and temperature will increase. Should the voltage/temperature combination enter Region II, the charge controller will sense the condition and act in such a manner as to maintain the operating condition of the battery within this region. Since the charge controller may operate directly on charge current and on other parameters only as a function of charge current, the circuitry was designed to vary the current in order to maintain operation in Region II.

Within Region II, the charge controller becomes essentially a voltage regulator with an output voltage related to temperature. Figure V-3 illustrates this mode of operation.

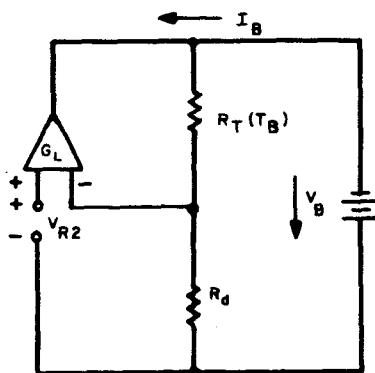


Figure V-3. Charge Controller Operation in Region II Functional Diagram

If the gain, G_L , is high, then it may be shown that

$$V_B = V_{R2} \left(1 + \frac{R_1}{R_d} \right),$$

where:

G_L = Effective transconductance of transistor circuitry in Region II,

V_B = Battery voltage,

V_{R2} = Reference voltage for voltage/temperature,

R_d = Constant resistance, and

R_t = Temperature sensitive resistor with a negative temperature co-efficient.

As the battery temperature increases, R_t decreases, thereby reducing the value of V_B at which the circuit will regulate.

4. REGION III OPERATION

In Region III, the charge controller operates as a constant current regulator in essentially the same manner as in Region I, with the exception that the regulated current is the trickle charge current. There are two conditions which could lead to operation in Region III.

The first condition would occur in Region II operation if battery voltage and temperature conditions forced the voltage/temperature circuit to reduce charging current to the trickle charge limit.

The second condition would occur should the battery pack temperature rise to the high-temperature limit indicated in Figure V-1. In this case, the circuitry designed to detect this high-temperature condition would immediately reduce charge current to the trickle rate. Should the temperature decrease by a small, predictable amount, the charge current will be increased to a level determined by the current regulator and the voltage/temperature sensing circuits. If, after the higher charge current level is restored, battery dissipation could be high enough to cause the high-temperature limit to be reached, a cyclical condition might be established. Essentially, in this mode of operation, the charge controller acts as a temperature regulator, and controls battery power dissipation in order to regulate battery temperature.

Charge controller operation in this mode (Region III) is shown in Figure V-4. The battery temperature (T_B) is sensed by thermistor, T , and resistor, R_S , which act as a half-bridge. The voltage, V_T , reaches the trip level of the Schmitt Trigger circuit at the high-battery temperature due to the negative temperature coefficient of the thermistor. At the trip level, the Schmitt Trigger delivers a step current to the current regulator which causes the battery current, I_B , to be reduced to the trickle-charge level. As the battery temperature decreases, V_T will decrease by an amount equal to the hysteresis of the Schmitt Trigger circuit.

Upon reaching the lower trip level, the Schmitt Trigger will change state and allow the current regulator to charge the battery at the normal rate.

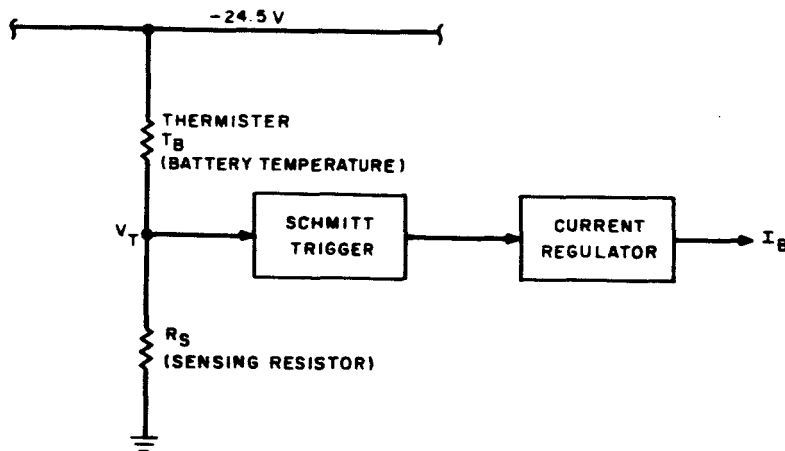


Figure V-4. Charge Controller Operation in High-Temperature Limit Mode (Region III)

C. TELEMETRY CIRCUITS

The battery module electronics will provide nominal analog signals for the spacecraft telemetry subsystem as indicated in Table V-1. All telemetry circuits will be capable of operation as described in Table V-1 with a maximum output impedance of 3000 ohms.

D. GROUND COMMANDS

For purposes of protection against various possible failure modes and for flexibility of load programming, two ground commands are included. One command protects against failure in the temperature and voltage circuits by providing a trickle-charge override.

TABLE V-1. BATTERY ANALOG SIGNALS FOR TELEMETRY SUBSYSTEM

Parameter	Parameter Range	Nominal T/M Signal Range
Battery Voltage Battery Temperature Battery Charge Current Battery Discharge Current	To be added	0 to -6 volts* -6 volts max.* -0.5 to -6 volts* -0.5 to -6 volts*
* Will require calibration curves		

Implementation of this scheme is shown in Figure V-5. Here, the trickle-charge override, derived from the electronics module, disables the temperature and voltage sensing circuits at their point of connection to the current regulator loop by merely blocking their outputs. This disable function will be in effect so long as a -23.5-volt signal is maintained at this control input.

The function of the second ground command is to disconnect a battery from the subsystem. There are sixteen commands available for this purpose (two for each battery module) so that individual batteries may be removed and reconnected as required.

The configuration for this scheme is shown in Figure V-6.

Here, the ground command signal, via the electronics module, activates a relay with both sets of contacts in series with the battery. The relay disconnects the negative terminal of the battery from the subsystem. This disconnection will be in effect until another ground command is sent to switch the relay contacts back to their original position.

Only the battery voltage telemetry and sensing divider ($V_B - V_T$) remain across the battery at all times. These two circuits are resistive voltage dividers with very small power dissipation levels.

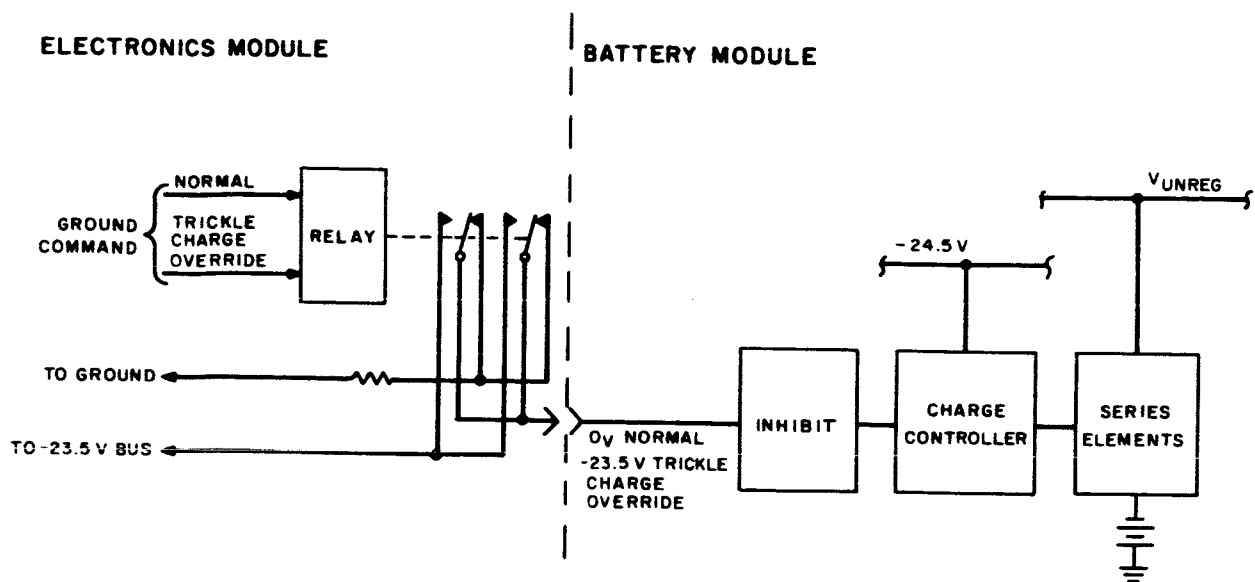


Figure V-5. Trickle-Charge Override Functional Diagram

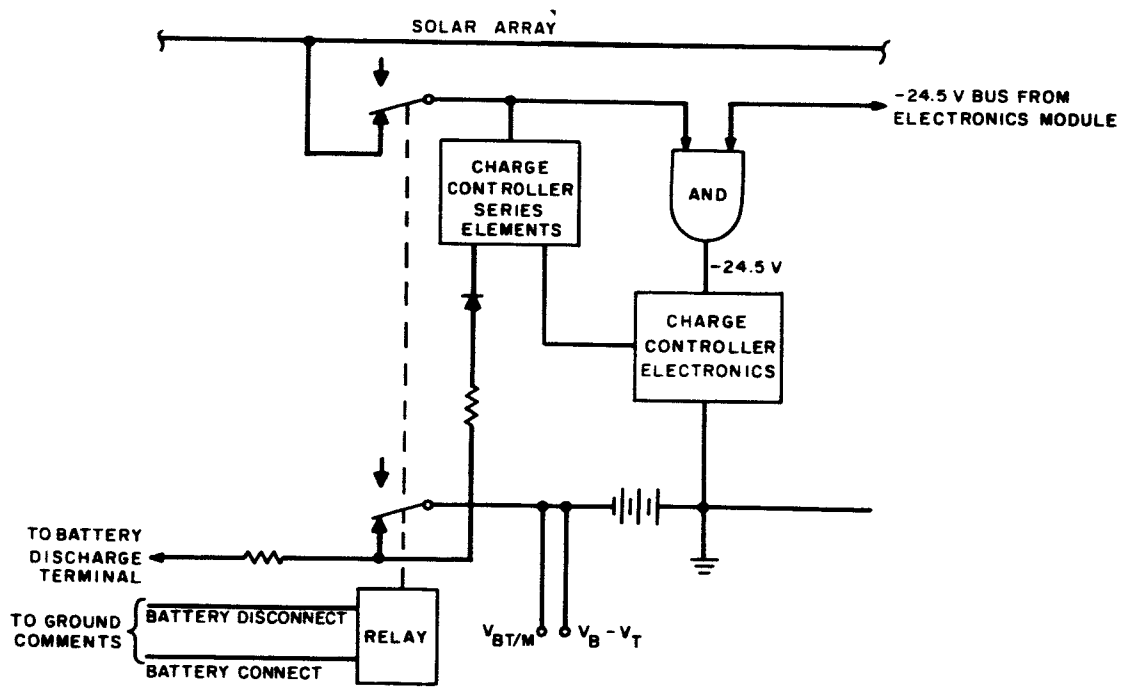


Figure V-6. Battery Disconnect Functional Diagram

SECTION VI

ELECTRONICS MODULE

A. ELECTRICAL DESIGN

The electronics module contains two redundant pulse-width modulated (PWM) voltage regulators, the regulated bus comparator, eight battery discharge diodes, two auxiliary regulators, the shunt regulator sensing and amplifying circuit, and the telemetry and ground-command circuits.

The constant-frequency PWM regulator was developed under AVR Contract NAS5 - 3248 and is described in the Final Report on that contract, dated July 31, 1964.

A new breadboard model has been assembled and is currently being used for preliminary radio-frequency interference (RFI) testing.

B. MECHANICAL DESIGN

1. GENERAL

The electronics module packaging concept and component arrangement has been completed. The module will consist of two 4 x 6 x 13-inch machined aluminum sections joined to form an 8 x 6 x 13-inch housing (4 by 4 eight tab full C dimension). The package is divided generally into an RFI compartment containing the -24.5-volt regulator switching and energy storage networks, a printed circuit board compartment containing all of the low-level control circuitry and a common harness compartment (see Figure VI-1). RCA irridite finish 1980135 (meeting specification MIL-C-5541) is proposed for both interior and exterior surfaces of the module.

2. PRINTED-CIRCUIT BOARDS

The printed-circuit-board compartment will contain five single-sided boards presently containing the following circuitry:

- a. -24.5-Volt Regulator Control circuitry - 1 board for each redundant circuit;
- b. Regulated Bus Comparator circuitry - 1 board.

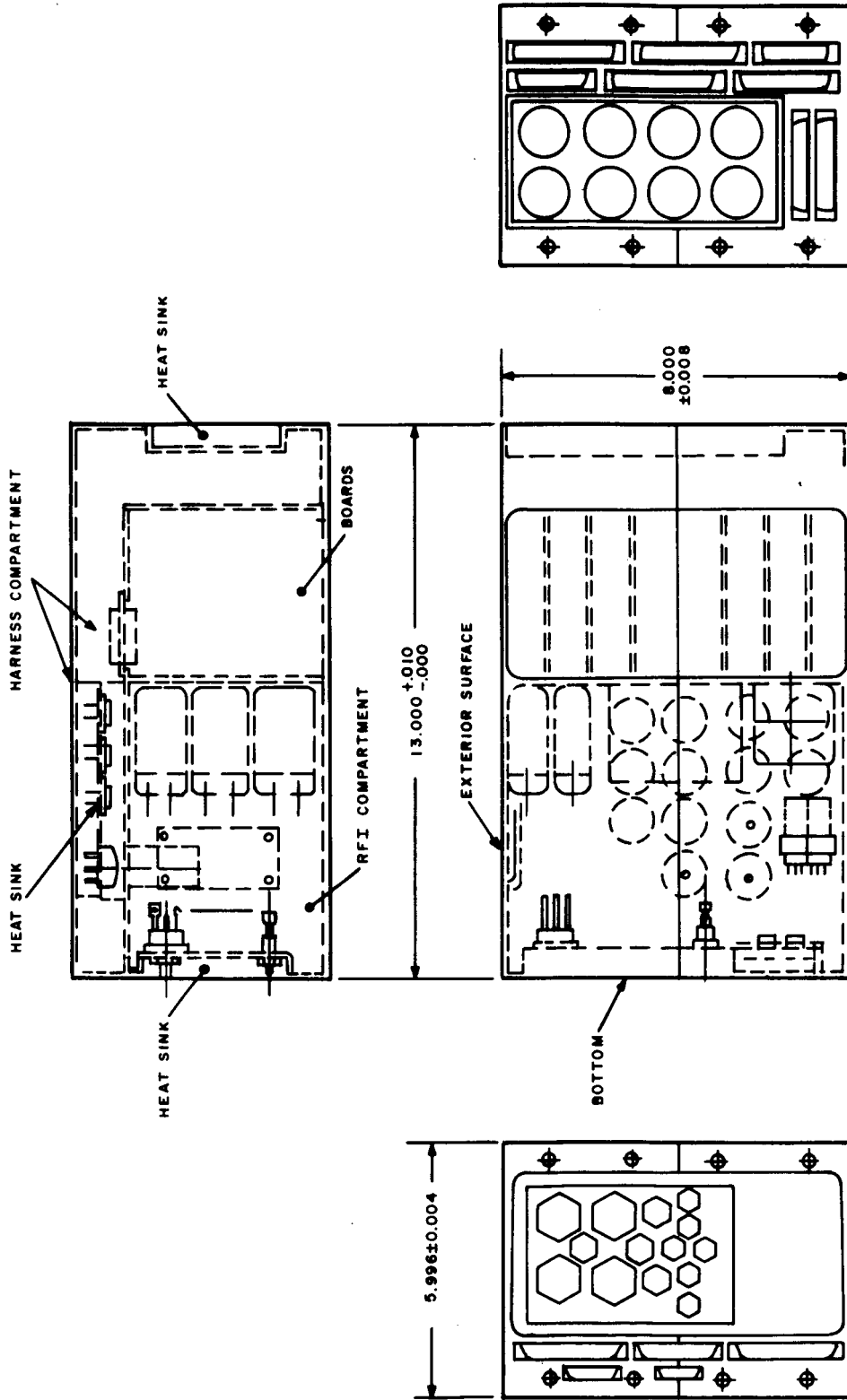


Figure VI-1. Proposed Nimbus-B Electronics Module Configuration

- c. -23.5-Volt Auxiliary Regulator circuitry (2 circuits), and Trickle Charge Override Relay circuitry - 1 board; and
- d. Shunt-Regulator Amplifier and Current Telemetry circuitry - 1 board.

In addition to the above boards, it is proposed to also mount two fuse boards, each capable of containing 25 fuses, within this compartment.

3. CONNECTORS AND WIRING

The Cannon gold-plated series D connectors are proposed for use on all external box connectors. The Burndy Corporation type UPC connectors are proposed for use as printed-circuit-board connectors.

Preliminary external module connector assignments have been made as follows:

- a. Module top (array side):
 - (1) four 50-pin connectors - Spacecraft regulated loads and returns;
 - (2) one 50-pin connector - Spacecraft unregulated loads and returns;
 - (3) one 25-pin connector - Solar array input (flight);
 - (4) one 25-pin connector - Solar array input (ground checkout); and
 - (5) one 50-pin connector - minus 24.5 V and 23.5 V to battery modules.
- b. Module bottom (earth side):
 - (1) one 50-pin connector - Battery module discharge and return;
 - (2) one 50-pin connector - Battery module connections for charge, shunt limiter, and trickle charge override;
 - (3) one 25-pin connector - Telemetry signals and returns;
 - (4) one 15-pin connector - Electronics module test points; and
 - (5) one 9-pin connector - Ground command signals.

Internal module wiring will be accomplished in a harness compartment which will be completely accessible through a removable module cover. Interconnecting wiring will be formed into a pre-wired harness including the harness board for printed circuits, module connectors, and umbilical wires. A major portion of the wiring can be done outside the module with unit-assembly wiring kept to a minimum.

4. ELECTROMAGNETIC COMPATIBILITY

Preliminary electromagnetic interference (EMI) investigations have been completed on the electronics module breadboard circuits, and the packaging configuration has been reviewed by an EMI consultant. The isolation of the regulator switching and storage networks, and consequent filtering of all wiring entering or leaving these circuits, will greatly reduce the electromagnetic interference generated. Tentative filter designs have been selected and an EMI Control and Test Plan is presently being written.

5. WEIGHT

The total estimated weight of the electronics module at the present time is 20.00 pounds. This is broken down as follows:

a. Housings, covers, and heatsinks	-	5.08 lbs
b. Board material, connectors, mtg. slides, and misc. hardware and brackets	-	2.70 lbs
c. Electronic parts and filters	-	11.22 lbs
d. Harness wire and conformal coating	-	1.00 lb
		<hr/>
	TOTAL:	20.00 lbs